Canadian Technical Report of
Hydrography and Ocean Sciences 230

2003

Modelling the tides of the Bras d'Or Lakes

by

F. Dupont, B. Petrie and J. Chaffey

Ocean Sciences Division
Maritimes Region
Department of Fisheries and Oceans
Bedford Institute of Oceanography
P.O. Box 1006
Dartmouth, Nova Scotia
Canada B2Y 4A2

Cat. No. Fs 97-18/230 ISSN 0711-6721

Correct citation for this publication :

Dupont, F., B. Petrie and J. Chaffey. 2003. Modelling the tides of the Bras d'Or Lakes. Can. Tech. Rep. Hydrogr. Ocean Sci. 230: viii + 53 pp.

TABLE OF CONTENTS

LIST OF FIGURES

LIST OF TABLES

ABSTRACT

Dupont, F., B. Petrie and J. Chaffey. 2003. Modelling the tides of the Bras d'Or Lakes. Can. Tech. Rep. Hydrogr. Ocean Sci. 230: viii + 53 pp.

The results of a finite element tidal model for the Bras d'Or Lakes are presented and compared to existing sea level and current data for the five major constituents (M2, S2, N2, K1 and O1). The amplitudes and phases of elevation agree to within 0.02 m and 20^o throughout the Lakes with the largest discrepancies in the Great Bras d'Or Channel. The M2 modelled currents and phases match the observations at the mouth of the Great Bras d'Or Channel where the measured flow exceeds 1 m/s. For the other constituents the modelled and observed currents are within 0.08 m/s and 45^o; the greatest discrepancies are for the diurnal components. In Barra Strait, the area with the strongest flows after the Great Bras d'Or Channel, the agreement between observed and modelled currents is poor. This is particularly true for M2 where observed tidal flows were nearly 0.5 m/s greater than modelled currents. The uncertainty in the location of the moorings could account for some of the disagreement.

Dupont, F., B. Petrie and J. Chaffey. 2003. Modelling the tides of the Bras d'Or Lakes. Can. Tech. Rep. Hydrogr. Ocean Sci. 230: viii + 53 pp.

RÉSUMÉ

Les resultats d'un modèle d'éléments finis de marée pour les lacs Bras d'Or sont présentés and comparés à des observations d'élévation and de courantomètre pour les cinq constituantes majeures (M2, S2, N2, K1 et O1). Les amplitudes et les phases de l'élévation sont en accord à près de 0.02~m et 20 degrés partout au travers des lacs avec les plus larges différences dans le chenal du Grand Bras d'Or. Les courants M2 du modèle et les phases associées sont en accord avec les observations à la tête du chenal du Grand Bras d'Or là où les vitesses mesurées dépassent 1~m/s. Pour les autres constituantes, les courants observés et ceux du modèle sont en accord à près de 0.08~m/s et 45 degrés; les plus grandes différences provenant des composantes diurnes. Dans le détroit de Barra, la région des plus forts courants après le chenal du Grand Bras d'Or, l'accord entre les courants observés et ceux du modèle est médiocre. Ceci est particulièrement vrai pour M2 où les courants observés dû à la marée sont de près de 0.5~m/s plus grands que ceux du modèle. L'incertitude dans la position des mouillages peut expliquer une partie de ces différences.

1. Introduction

The Bras d'Or Lakes are connected to Sydney Bight and the Atlantic Ocean by a 30 km long, narrow, shallow passage, the Great Bras d'Or Channel (Fig. 1). The channel has an average width of about 1.3 km, an average depth of about 19.5 m and a maximum depth of 95 m. The most severe restriction is at the mouth of the channel where it opens onto Sydney Bight. There the width is only 320 m, the maximum depth is 16.2 m, and the cross-sectional area is 2400 m^2. Most of the water exchange between the Lakes and the ocean must occur through this small opening.

The 8 km long Little Bras d'Or Channel, the only other permanently open connection to the ocean, is even more restrictive. It is less than 100 m wide and 5 m deep on average. It does not appear to play a major role in the temperature and salinity distributions in the Lakes (Gurbutt and Petrie, 1995). A lock on St. Peter's Inlet on the southern side of Bras d'Or Lake is opened occasionally to allow vessels to enter or leave the Lakes.

The interior of the Lakes consists of several interconnected basins and channels with a maximum depth of 280 m in St. Andrew's Channel. Two passages of note are Barra Strait which controls the exchange between the North Basin and Bras d'Or Lake, and Little Narrows which separates Whycocomagh Bay from St. Patrick's Channel. The Lakes have a shoreline of about 1000 km excluding islands (from 1:50 000 digital charts), total surface area of about 1.07 billion m^2, and a volume of approximately 32 billion m^3. A review of the general physical oceanography of the Lakes was given by Petrie and Bugden (2002).

The restricted opening to Sydney Bight is a major factor influencing the tidal circulation in the Bras d'Or Lakes. Petrie (1999) noted that the amplitudes and phases of the major tidal constituents (M2, S2, N2, K1, O1) change rapidly in the Great Bras d'Or Channel. For example, the amplitude of the major constituent, M2 (principal lunar component), decreases from about 0.37 m outside the mouth of the Lakes to about 0.04 m in the North Basin. The M2 phase changes by about 75 degrees along the Channel. Inside the Lakes and based on 5 tidal records, the M2 amplitude increases slightly from North Basin through Barra Strait into Bras d'Or Lake by about 0.005 m. The phase in Bras d'Or Lake lags the phase at the mouth of Great Bras d'Or Channel by about 130 degrees. A short record, 21d, from the western end of Whycocomagh Basin indicates that there are no semidiurnal or diurnal tides detectable. M2 tidal currents in Great Bras d'Or Channel and in Barra Strait ranged from about 0.5 to 0.8 m/s based on current meter data from the early 1970s. Gurbutt and Petrie (1995) showed that the tidal flows were important contributors to mixing in the Lakes and consequently influencing their temperature and salinity distributions.

Petrie (1999) developed a 1 dimensional, cross-sectionally averaged model of sea level variability in the Lakes. This model showed the importance of frictional dissipation in the Lakes, particularly in the narrow passages in Great Bras d'Or Channel and Barra Strait. The model incorporated the major basins of the Lakes as straight sided boxes of constant depth, with surface area and volume equivalent to the Lakes' basins. Although crude, the model produced results that were in good agreement with the available tidal and non-tidal sea level observations in the Lakes.

In this report we develop a 2 dimensional, depth-averaged, finite element model (Dupont et al., 2002) of the tidal circulation in the Lakes incorporating realistic topography and having 8614 nodes. Five tidal constituents (M2, S2, N2, K1 and O1) are considered. All constituents were run simultaneously and separated afterwards by harmonic analysis. Tides were specified on the outer boundary in Sydney Bight based on model solutions for the east coast region (Dupont et al., 2002 and available on the Ocean Sciences Division website located at http://www.mar.dfo-mpo.gc.ca/science/ocean/coastal_hydrodynamics/WebTide/webtide.html). Besides presenting the results for the Lakes as a whole, we focus on the tides in the Great Bras d'Or Channel, Barra Strait and Denys Basin. The first 2 areas are where major dissipation and strong tidal currents occur. Denys Basin is an area of prime oyster reproduction and the focus of a major effort by the Oceans Sector of DFO.

2. Tides in the Bras d'Or Lakes

2.1 The entire domain

The depths for the Lakes used in the model are based on the contoured isobaths and spot measurements from the Canadian Hydrographic Service charts 4277, 4278 and 4279 (Fig. 2a). The deep areas in St. Andrews Channel (to 280 m), the North Basin (to 229 m) and Bras d'Or Lake (to 119 m) are notable. Denys Basin is a shallow (<12 m) isolated feature on the western side of the Lake and is joined to the Lake by a ~3 km long, 180 m wide channel. In our model the only connection to the ocean is the Great Bras d'Or Channel. The Little Bras d'Or Channel was closed to control numerical instability that developed in this region. While the tidal flows in this Channel are known to be strong (Gurbutt et al., 1993), its influence on the Lakes as a whole are small (Gurbutt and Petrie, 1995). The finite element mesh is shown in Figure 2(b).

The results of the model runs for the 5 major tidal constituents are shown in Fig. 3 as a colour maps for elevation and white lines every 20 degrees for phase. The M2 elevation decreases rapidly along the Great Bras d'Or Channel with most of the attenuation occurring between Carey Point at the mouth and the Seal Island Bridge, about a third of the way towards the Lakes. In this region, the elevation falls from about 0.35 to 0.15 m. Inside the Lakes, the elevation is

between ~0.025 and 0.05 m in all areas, even in Whycocomagh Basin where no observed tide was recorded. The phase of the tide shows changes in increments of 20 degrees along the Great Bras d'Or Channel, in Barra Strait and Denys Basin. Another interesting feature outside the Lakes is the decreased amplitude seen in St. Ann's Bay, the smaller basin to the north of Great Bras d'Or Channel. The entrance to St. Ann's Bay is restricted by a sand and rock spit that nearly closes off its mouth.

Outside the Lakes, the S2 constituent has an amplitude of about 0.1 m (Fig. 3, Table 1). It decreases along the Great Bras d'Or Channel to about 0.01 m in the inner basins. This decrease by a factor of about 10 is similar to the reduction seen for M2. Significant changes of phase also occur in the Channel and in Barra Strait.

The N2 constituent at 0.076 m in Sydney Bight is the smallest of the principal semidiurnal components. Its variations in amplitude and phase are similar to those of M2 and S2. One notable feature is the larger amplitude in the central part of St. Patrick's Channel relative to Whycocomagh and Baddeck Bay (Fig. 3). This is caused in part by the very restricted passage between the western end of the Channel and Whycocomagh Bay.

The 2 diurnal constituents, O1 and K1, have comparable amplitudes outside the Lakes, about 0.08 m, and respond similarly as they move into the Lakes (Fig. 3). The observed amplitude ratios relative to North Sydney are approximately 0.2 in North Basin and Bras d'Or Lake, whereas, the semidiurnal constituents are reduced to about 0.1 of their values outside the Lakes (Table 2). This indicates that the dissipation is frequency dependent and is greater for the higher frequency components (see Petrie, 1999).

Comparisons of the model and observations of amplitude and phase for selected locations in the Lakes (Fig. 1, Table 2) are shown in Fig. 4-8. In these comparisons, we have used the harmonic amplitudes and phases for Baddeck to represent the middle of North Basin and Eskasoni to represent the Bras d'Or Lake. Note that there is little difference among the tidal constants for Bras d'Or Lake (Table 2). We have selected the longest records for the comparisons of Fig. 4-8. The model is generally within a couple of centimetres of the observed amplitudes for M2 and 1 cm for the other constituents. The phases generally agree to within 20 degrees.

Another comparison of the data including all harmonics given in Petrie (1999) is shown in Fig. 9. The largest discrepancies are for harmonics for Black Rock Point, based on a short, 20 d sea level record.

The currents for each tidal constituent at 6 stages of the tide are shown in Fig. 10-14. The 0/6 cycle corresponds to high tide at North Sydney, the 3/6 cycle to low tide. The strongest inflows to the Lakes for M2 occurs during high tide and for about 2 hours after high tide (Fig. 10). The strongest flows are found in the Great Bras d'Or Channel and in Barra Strait. In a similar fashion, the strongest outflows occur for low tide at North Sydney and for about 2 hours following low tide. Currents for the S2 and N2 components are considerably weaker but behave in a similar fashion (Fig. 11, 12). The peak strength of the diurnal currents is about the same as that for S2 and N2 with again a similar time variation as M2 (Fig. 13, 14).

2.2 Great Bras d'Or Channel

The bathymetry and mesh used in the model are shown for the Great Bras d'Or Channel in Fig. 15. The initial third of the Channel abutting Sydney Bight is generally shallower than the remaining portion. It also features the narrowest section which is located at the mouth. The amplitude and phase variations for the 5 tidal constituents are shown in Fig. 16. The M2 amplitude undergoes most of its decrease, >0.3 m to 0.05 m, between the mouth of the Channel and Seal Island. Most of the phase change of 60^{o} occurs in the last third of the Channel. Similar variations are seen for the other tidal constituents.

The current variations along the Channel for all constituents are shown in Fig. 17-21. These show considerably more detail than was shown in the plots that included the entire Lakes. The role of the cross-sectional area in determining the strength of the flow is evident in these figures - the deep area midway along the Channel features the weakest flows; the mouth and Seal Island areas, where the Channel is constricted, has the largest currents. The pattern for the other tidal components is similar but with greatly reduced current strengths.

Currents were extracted for 2 model points: one at Carey Point near the mouth of the Channel, and the second at Seal Island about one third of the way along the Channel from the mouth (see Fig. 16 for locations). The time series of currents was analyzed for tidal amplitudes and phases and the results (major axes) are shown in Fig. 22 for Carey Point. An ADCP was deployed off Carey Point for 6 months. Strong currents moved the mooring off site and it appears that a maximum of 21 d of data were collected at the original mooring location. It is not possible to determine the position of the mooring with any accuracy after the initial 21 d. The acoustic reflection from the surface indicates that the mooring was moved into deeper water and that it was displaced several times resulting in depth changes of up to a few meters. The analysis of this record is therefore somewhat in doubt. In spite of this, we show the tidal analysis of the currents for 3 depths, 4.5, 9.5 and 18.5 m along with the model results (Table 3, Fig. 22). The observed and modelled M2 tidal harmonics agree. The S2 modelled tide had an amplitude ratio of ~0.7 of the observed current and lagged

it by about 10^o (20 minutes). The largest discrepancies were for the diurnal constituents: the modelled K1 amplitude was a factor of 0.6 of the observed, the phase was later by about 20^o (80 minutes); the amplitudes for O1 were in agreement, however, the phase of the modelled tide was later by about 40^o (170 minutes). Note that the record length was too short to extract N2 currents without inference.

In addition to the finite element model of the entire Lakes, we examined a local model based on sea level differences for Sydney Bight (we chose the North Sydney constants) and Big Bras d'Or (Table 2). The balance is among acceleration, pressure gradient and linearized friction. To calculate the pressure gradient a distance of 4 km was used. This was chosen on the basis of a tidal analysis, with constants much like North Sydney, of a short sea level record from Table Head Point, a site about 4 km from Big Bras d'Or. The linearized friction coefficient was chosen by adjusting it to get the correct amplitude for M2. Table 3 shows that the local model gets similar results for the tidal currents as the finite element model but with slightly later phases for all constituents and higher amplitudes except for M2. Comparing the balances of acceleration and pressure gradient alone, and friction and pressure gradient, indicates that friction dominates, giving almost the same result as the combined model.

The model tidal currents are reduced off Seal Island compared to the flows at Carey Point (Fig. 23). Note though that there is no apparent phase difference of modelled harmonic constituents between the 2 sites. This was also noted by Petrie (1999) for his model of M2 and is also predicted from theoretical considerations (Vennel, 1998). There were moorings in the Seal Island area in 1973 and 1974. The positions of these moorings is uncertain as the mooring logs puts one of them (1974) onshore. However, the bottom depths of the moorings places them in a deep area to the southwest of Seal Island. The semidiurnal flows estimated from these data are about 0.2 m/s, considerably less than the model flows in the narrows at Seal Island. The position of the moorings is too uncertain to compare observed and modelled currents.

The tidal flows at the mouth near Carey Point are the strongest in the Lakes. Fig. 24-28 focus on this area and present the model flows at 6 stages of the tides at North Sydney beginning with high tide (0/6 cycle). Because the flows, especially M2, are so strong, they can generate a residual circulation through both the advective and the quadratic friction terms. The residual flow and flow times model depth were derived from the mean current at each nodal point over the 36 d simulation (Fig. 29). Note that all grid points are not shown, therefore there is an apparent net flow into the Lakes. Some grid points in the narrowest part of the channel with mean flows towards Sydney Bight are not displayed to reduce the clutter in the figure. The residual circulation features a strong (~0.1 m/s) cyclonic gyre outside the mouth of the Lakes and a weak cyclonic gyre

beginning as the channel widens just inside the mouth (Fig. 29). The evidence of a strong residual flow also implies that there should be substantial tidal harmonics generated by the same terms in the momentum equations. In fact, the analysis of the observed tidal currents shows that a number of the shallow water constituents have amplitudes of 0.05-0.1 m/s. The M4 component is generally the largest at the 3 depths the analyses were done, and ranges from 0.083 to 0.117 m/s.

2.3 Barra Strait

The second focus area is Barra Strait (Fig. 30) where strong tidal flows can lead to significant mixing (Gurbutt and Petrie, 1995). The tidal elevations and phases for the 5 leading constituents are shown in Fig. 31. All constituents show major changes of amplitude (~33%) and phase (up to ~40^{o}) at the Strait.

The tidal currents are shown at 6 stages of the tide for the 5 principal components in Fig. 32-36. The M2 amplitude is more than 4 times stronger than the next largest component, S2. The largest flows occur on the northeastern side of the Strait, near the location of the new causeway/bridge. This is close to the site where currents were measured in 1973 (5, 22 m for 30 d) and 1974 (5, 10, 20 m for 44 d) (Krauel 1975). The results from tidal analysis of these records and the model are shown in Fig. 37 and Table 4. The modelled semidiurnal amplitudes are within the ranges of the observed amplitudes but at the lower end. The modelled semidiurnal phases are also within the ranges. The observed ranges of amplitude and phase are large. The orientations of the modelled and observed flows agree to within a few degrees. The modelled diurnal amplitudes are slightly smaller than the lowest observed flow; the phase lags are slightly larger than the observed ones. The observed ranges of amplitude and phase are large. The orientations for the diurnal constituents are in excellent agreement. The positions of the moorings is probably accurate only to several hundred meters.

2.4 Denys Basin

Denys Basin is particularly interesting as it is a prime oyster spawning area and the focus of a number of initiatives carried out by the Oceans Branch of DFO. The bathymetry and mesh of the Basin are shown in Fig. 38. In the model the only connection to Bras d'Or Lake is through a long (~3 km), narrow (~180 m) channel that is generally about 10 m deep along its central axis.

The tidal elevations in the Basin are quite small with the largest, M2, having an amplitude of about 0.03m (Fig. 39). The amplitudes of S2, N2 and K1 are predicted by the model to be less than 0.01 m; the O1 amplitude is about 0.01 m. With such small elevations we expect that the tidal flows in the Basin will generally be weak. The current plots at 6 stages of the tides for the 5 constituents indicate that the largest flows in the Basin occur just inside the

western end of the entrance channel, between Martins and MacLean Points (Fig. 40-44). These flows peak at about 0.03 m/s for the M2 component. All of the water flowing into the Basin must come through the channel. Fig. 45 shows the currents over a tidal cycle for the 5 principal components at the point indicated in Fig. 39. Except for M2, which has a current amplitude of about 0.07 m/s, all components have amplitudes of less than 0.02 m/s. No current meter records have been collected in the Basin or in the channel connecting it to Bras d'Or Lake.

3. Summary

We have constructed a finite element model of the 5 principal tidal constituents in the Bras d'Or Lakes. The strongest flows (~ 1 m/s) are found in the Great Bras d'Or Channel near Carey Point and Seal Island, and in Barra Strait. Tidal currents in the Lakes as a whole are generally less than 0.1 m/s. The agreement between modelled and observed harmonics for elevation is generally to within a couple of centimetres and 20^o. The modelled currents have larger discrepancies with the percent error of the observed modelled amplitudes from the Great Bras d'Or Channel varying from 5% for M2 to 39% for K1. The error is defined as 100*(rms difference)/(average observed amplitude). The rms phase differences varied from 2^o for M2 to 43^o for O1. For Barra Strait the percent error for amplitudes ranged from 43% for S2 to 67% for O1; the rms phase differences varied from 15^o for M2 to 53^o for N2. In addition to the Great Bras d'Or Channel and Barra Strait, we focussed on Denys Basin. Tidal currents in Denys Basin were less than 0.03 m/s and elevations were less than 0.03 m. This implies that the tidal flushing of this region is weak.

3. Acknowledgements

We thank the Oceans Branch of DFO for financial support and D. Duggan (DFO, Oceans) for his encouragement and support of this work. We thank David Greenberg and Gary Bugden for useful internal reviews.

4. References

Dupont, F., C. Hannah, D. Greenberg, J. Cherniawsky and C. Naimie 2002. Modelling system for tides for the Northwest Atlantic coastal ocean. Can. Tech. Rep. Hydrogr. Ocean Sci. 221, vii + 72 pp.

Gurbutt, P. A., B. Petrie and F. Jordan 1993. The physical oceanography of the Bras d'Or Lakes: data analysis and modelling. Can. Tech. Rep. Hydrogr. Ocean Sci. 147: vii+61 pp.

Gurbutt, P. A. and B. Petrie 1995. Circulation in the Bras d'Or Lakes. Estuar. Coastal Shelf Sci. 41: 611-630.

Krauel, D. 1975. The physical oceanography of the Bras d'Or Lakes 1972-1974. Tech. Rep. 570, Fish. Mar. Ser., xii+357 pp.

Petrie, B. 1999. Sea level variability in the Bras d'Or Lakes. Atmos.-Ocean 37: 221-239.

Petrie, B. and G. Bugden 2002. The physical oceanography of the Bras d'Or Lakes. Proc. N. S. Inst. Sci. 42: 9-36.

Vennel, R. 1998. Oscillating barotropic currents along short channels. J. Phys. Oceanogr. 28: 1561-1569.

Table 1. Harmonic constants for the five principal tidal constituents (periods in h) at North Sydney. Note that the phases are referenced to Greenwich.

	Constituent					**Record Length (d)**
	M2 (12.42)	S2 (12.00)	N2 (12.63)	K1 (23.93)	O1 (25.82)	
Amplitude (m)	0.368	0.109	0.076	0.077	0.082	362
Phase (Greenwich)	353	37	330	325	287	

Table 2. Harmonic constants for the five principal tidal constituents (periods in h) at various locations in the Bras d'Or Lakes and their amplitude ratios (in brackets) and phase lags (in brackets) relative to North Sydney (Petrie, 1999). When more than one record was available from the same site, constants from the longer one are displayed. Note that the phases are referenced to Greenwich.

Amplitude (m) (Ratio)	**Tidal Constituent (period, h)**					**Record Length (d)**
Phase (Phase Lag)	M2 (12.42)	S2 (12.00)	N2 (12.63)	K1 (23.93)	O1 (25.82)	
Table Head	0.342 (0.93)	0.081 (0.74)	0.067 (0.88)	0.064 (0.83)	0.082 (1.05)	37
	353 (0)	41 (-4)	322 (8)	320 (5)	283 (4)	
Big Bras d'Or	0.165 (0.45)	0.033 (0.3)	0.035 (0.46)	0.038 (0.49)	0.032 (0.39)	47
	339 (14)	33 (4)	328 (2)	320 (5)	282 (5)	
Seal Island	0.073 (0.20)	0.011 (0.13)	0.016 (0.21)	0.012 (0.16)	0.014 (0.17)	42
	343 (10)	30 (7)	320 (10)	360 (-35)	305 (-18)	
Baddeck	0.037 (0.10)	0.010 (0.09)	0.009 (0.12)	0.015 (0.19)	0.015 (0.18)	34
	68 (-75)	121 (-84)	40 (-70)	68 (-103)	9 (-82)	
Iona	0.038 (0.103)	0.008 (0.07)	0.006 (0.08)	0.014 (0.18)	0.012 (0.15)	31
	77 (-84)	155 (-118)	58 (-88)	81 (-116)	354 (-67)	
Marble Mountain	0.046 (0.125)	0.006 (0.06)	0.007 (0.09)	0.018 (0.23)	0.017 (0.23)	35
	124 (-131)	183 (-146)	121 (-151)	58 (-93)	28 (-101)	
Johnstown Hbr.	0.045 (0.12)	0.007 (0.06)		0.016 (0.21)	0.017 (0.21)	22
	127 (-134)	205 (-168)		84 (-119)	31 (-104)	
Eskasoni	0.041 (0.12)	0.008 (0.07)	0.009 (0.12)	0.017 (0.22)	0.018 (0.22)	45
	121 (-128)	185 (-148)	91 (-121)	73 (-113)	25 (-98)	

Table 3. Tidal Current amplitudes (m/s), phases (Greenwich) and orientation at Carey Point

Depth (m)		M2	S2	N2	K1	O1
4.5	Amplitude	1.14	0.33		0.28	0.23
	Phase	192.5	222.2		123.3	67.3
	Orientation	45.6	48.7		40.4	41
9.5	Amplitude	1.24	0.38		0.30	0.25
	Phase	191.8	220.0		128.4	71.2
	Orientation	45.8	45.1		37.1	35.9
18.5	Amplitude	1.21	0.38		0.30	0.28
	Phase	190.4	218.6		124.5	68.1
	Orientation	42.7	43.5		42.0	39.5
Model	Amplitude	1.15	0.25	0.17	0.18	0.23
	Phase	193	231	162	145	112
	Orientation	52.5	50.8	50.9	48.7	50.1
Local Model	Amplitude	1.14	0.41	0.22	0.22	0.28
	Phase	202	237	169	159	119
Acceleration	Amplitude	3.7	1.28	0.73	1.23	1.82
Friction	Amplitude	1.2	0.43	0.23	0.22	0.28

Table 4. Tidal Current amplitudes (m/s), phases (Greenwich) and orientation at Barra Strait.

Depth (m)		M2	S2	N2	K1	O1
1973, 5m	Amplitude	0.55	0.15	0.11	0.10	0.09
	Phase	217	278	186	121	167
	Orientation	20	22	20	19	19
1973, 22m	Amplitude	0.31	0.06		0.06	0.06
	Phase	199	302		94	131
	Orientation	28	30		33	25
1974, 5m	Amplitude	0.79	0.11	0.10	0.13	0.14
	Phase	223	273	207	126	167
	Orientation	26	21	28	24	24
1974, 10m	Amplitude	0.58	0.11	0.13	0.15	0.13
	Phase	188	255	163	97	136
	Orientation	27	23	22	26	23
1974, 20m	Amplitude	0.45	0.08	0.04	0.10	0.10
	Phase	201	264	92	86	141
	Orientation	30	31	33	28	29
Model	Amplitude	0.32	0.07	0.05	0.05	0.04
	Phase	213	256	193	131	172
	Orientation	28	29	28	29	29

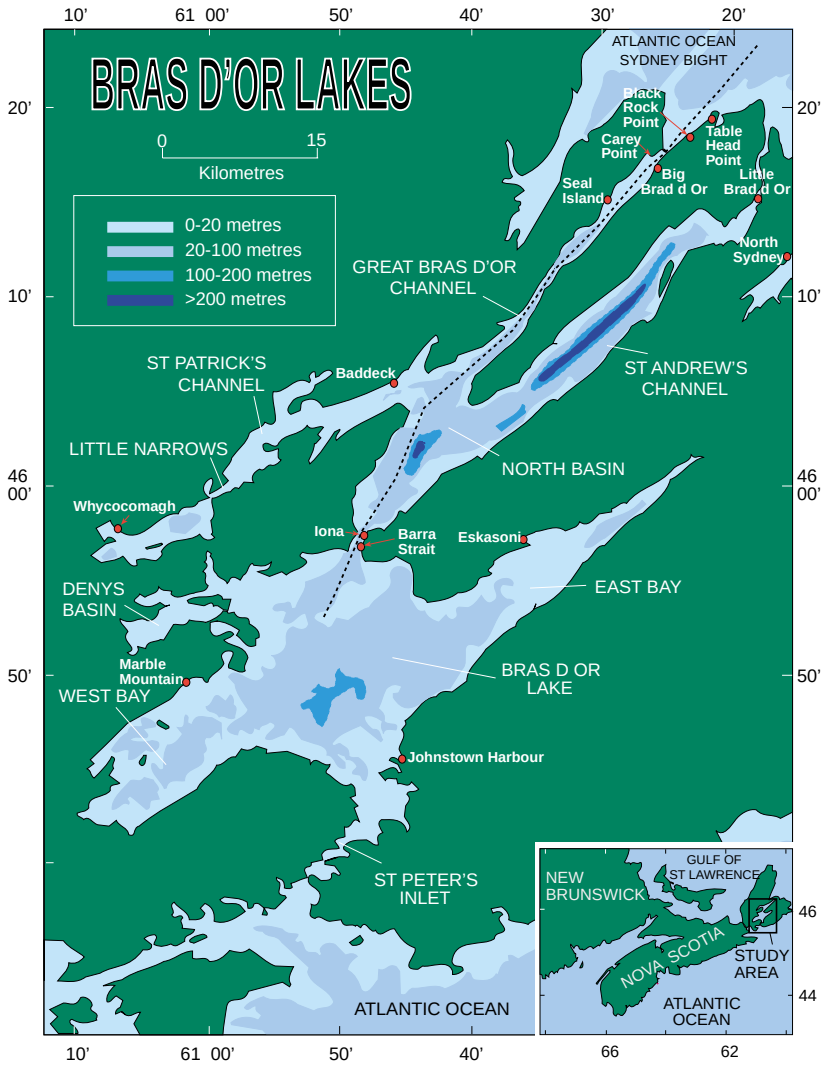

Figure 1. Bras d'Or Lakes with place names of locations used in the text. The broken line indicates where comparisons of observed and modelled tidal elevations are made.

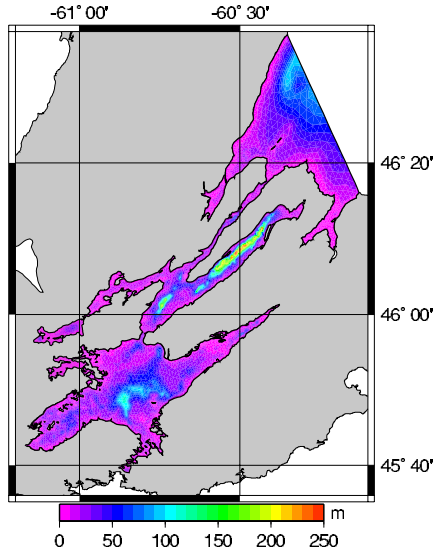

Figure 2(a). The model bathymetry for the whole computational domain.

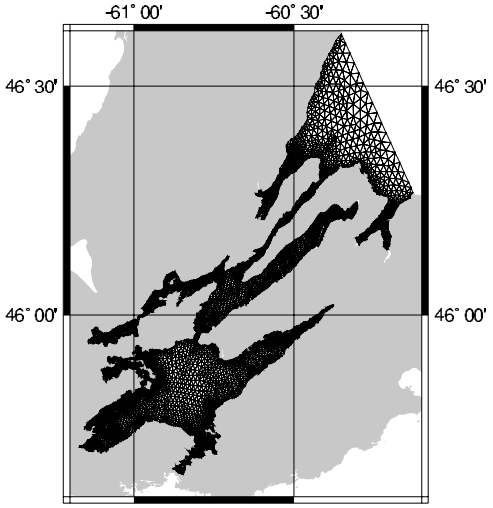

Figure 2(b). Finite element mesh of Bras d'Or Lakes model.

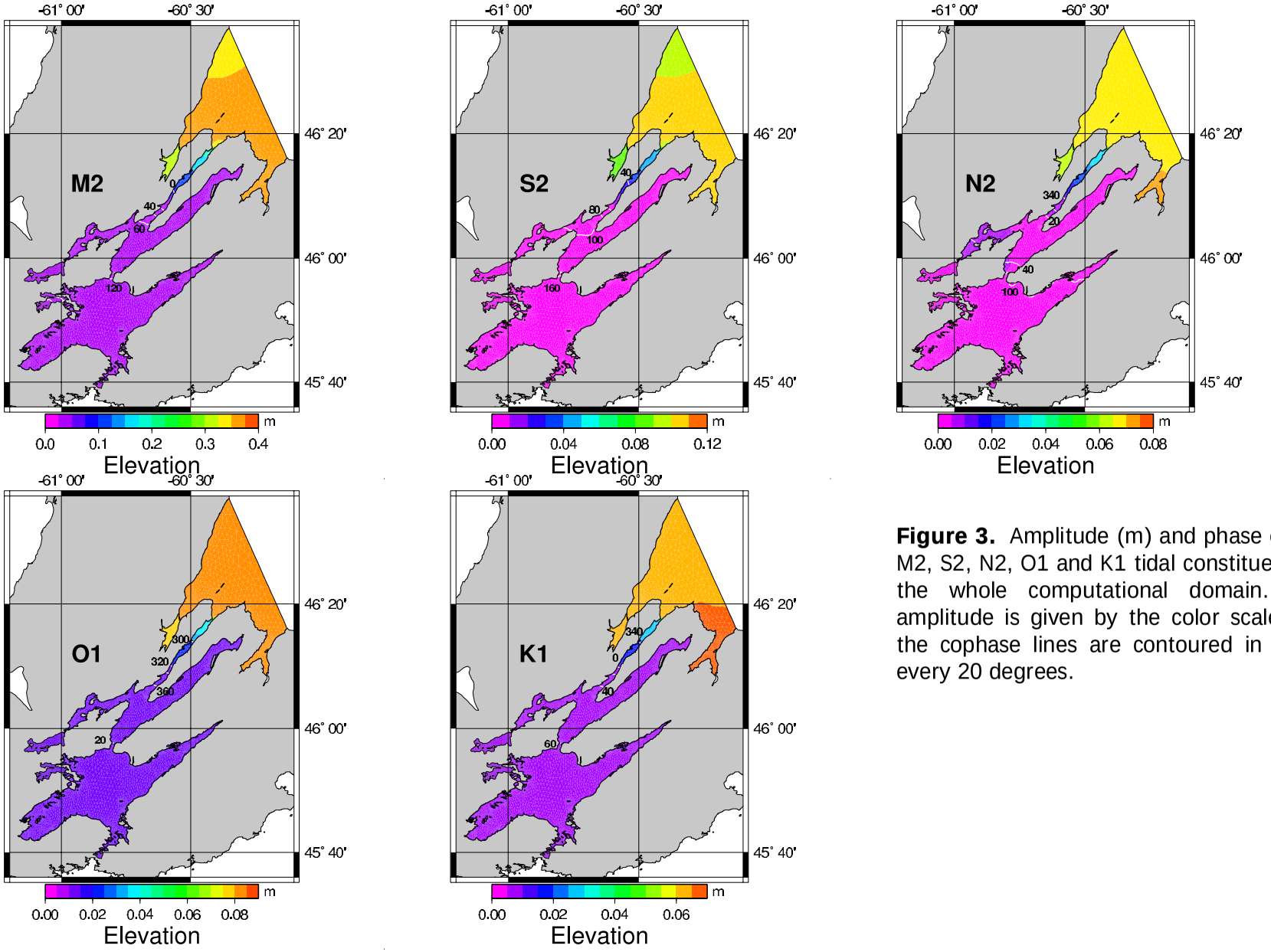

Figure 3. Amplitude (m) and phase of the M2, S2, N2, O1 and K1 tidal constituents in the whole computational domain. The amplitude is given by the color scale and the cophase lines are contoured in white every 20 degrees.

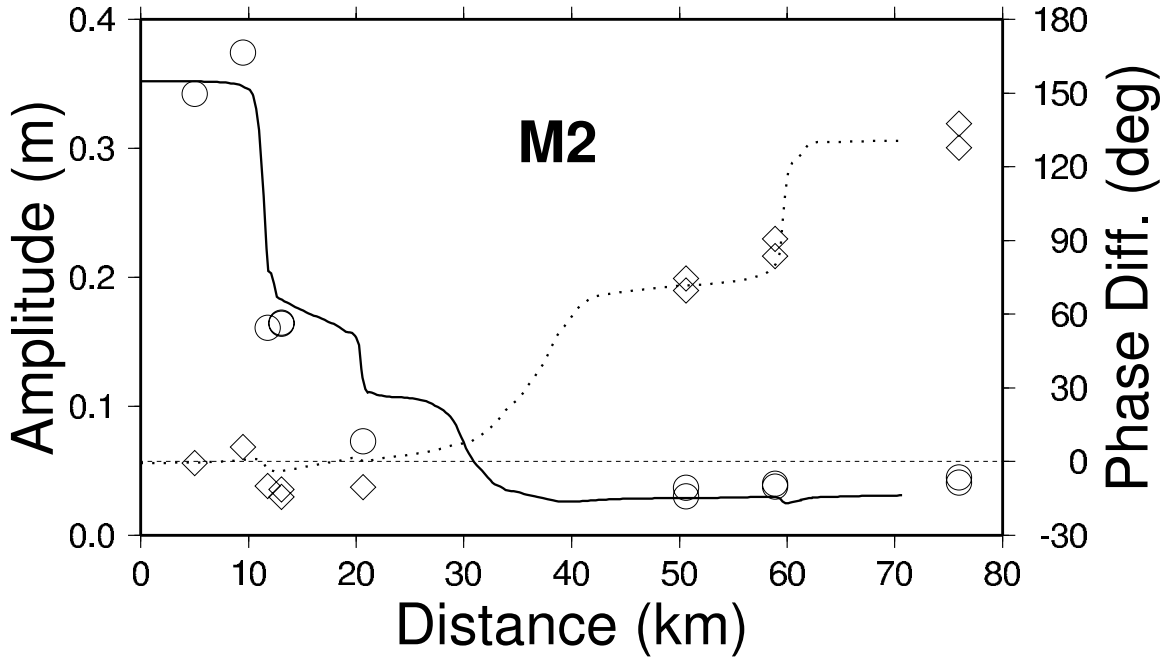

Figure 4. Amplitude (plain line) and phase (dotted line) for the M2 constituent along the line shown in Fig. 1. The observed harmonics are shown for comparison as open circles (amplitude) and open diamonds (phase). The thin dashed line shows the zero phase line.

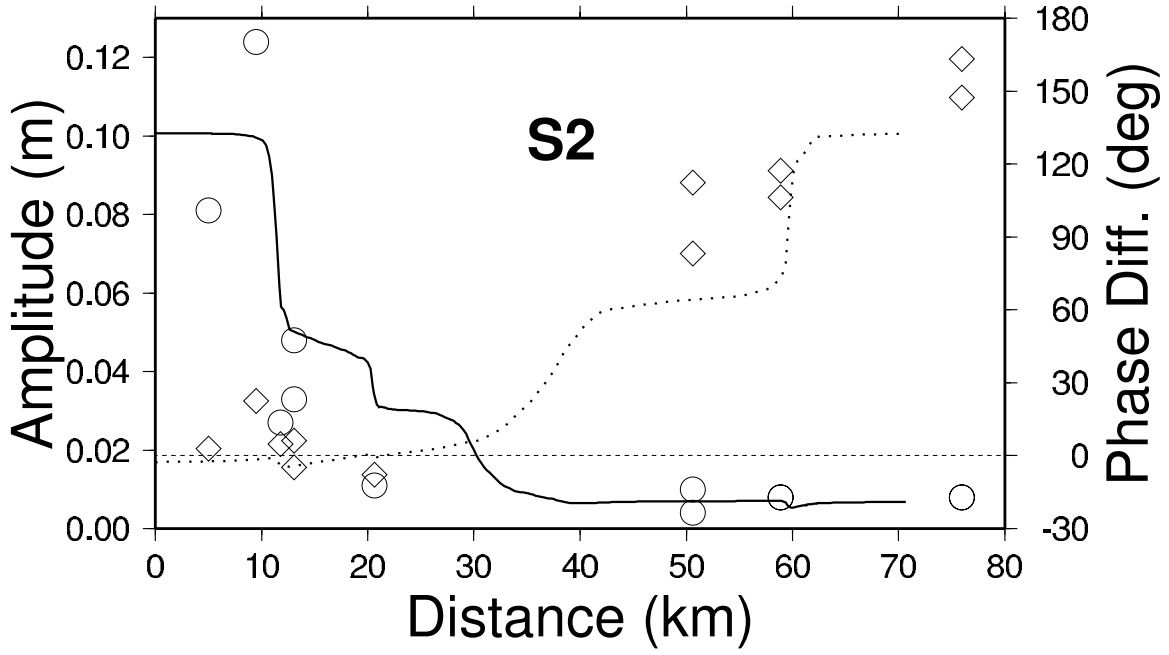

Figure 5. Amplitude (plain line) and phase (dotted line) for the S2 constituent along the line shown in Fig. 1. The observed harmonics are shown for comparison as open circles (amplitude) and open diamonds (phase). The thin dashed line shows the zero phase line.

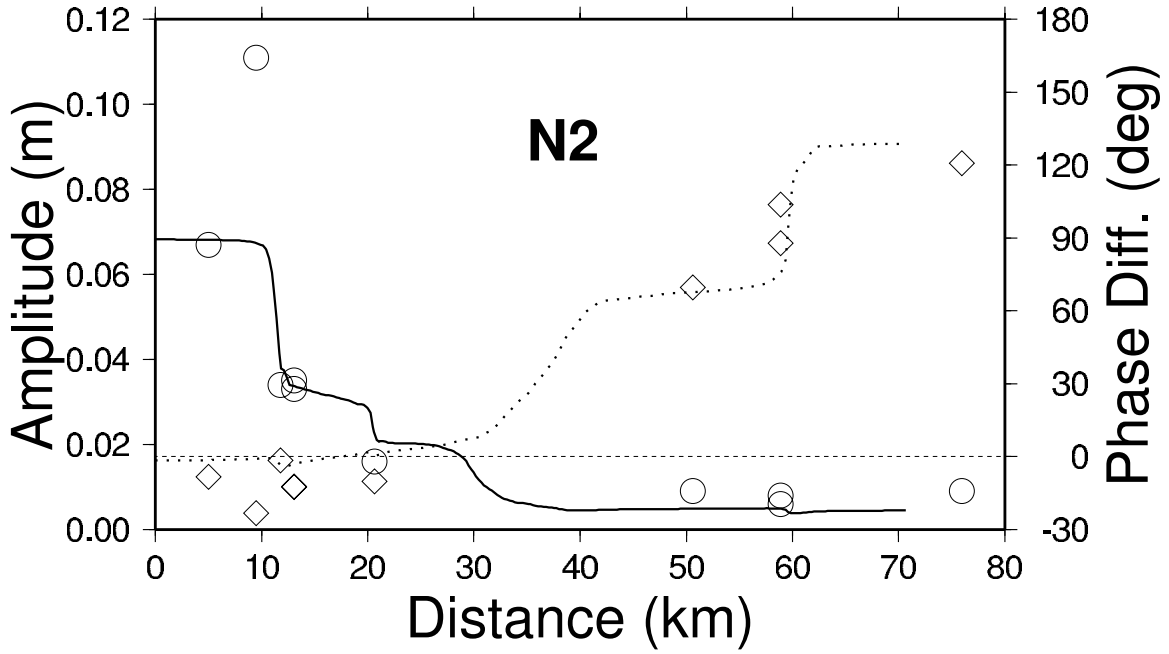

Figure 6. Amplitude (plain line) and phase (dotted line) for the N2 constituent along the line shown in Fig. 1. The observed harmonics are shown for comparison as open circles (amplitude) and open diamonds (phase). The thin dashed line shows the zero phase line.

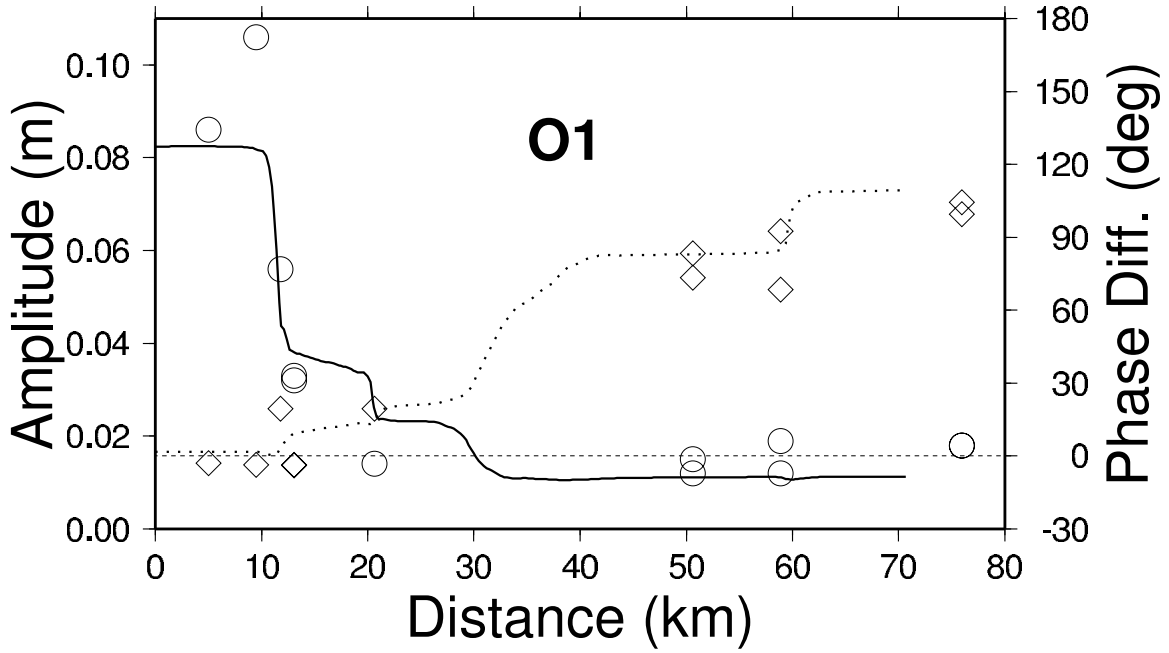

Figure 7. Amplitude (plain line) and phase (dotted line) for the O1 constituent along the line shown in Fig. 1. The observed harmonics are shown for comparison as open circles (amplitude) and open diamonds (phase). The thin dashed line shows the zero phase line.

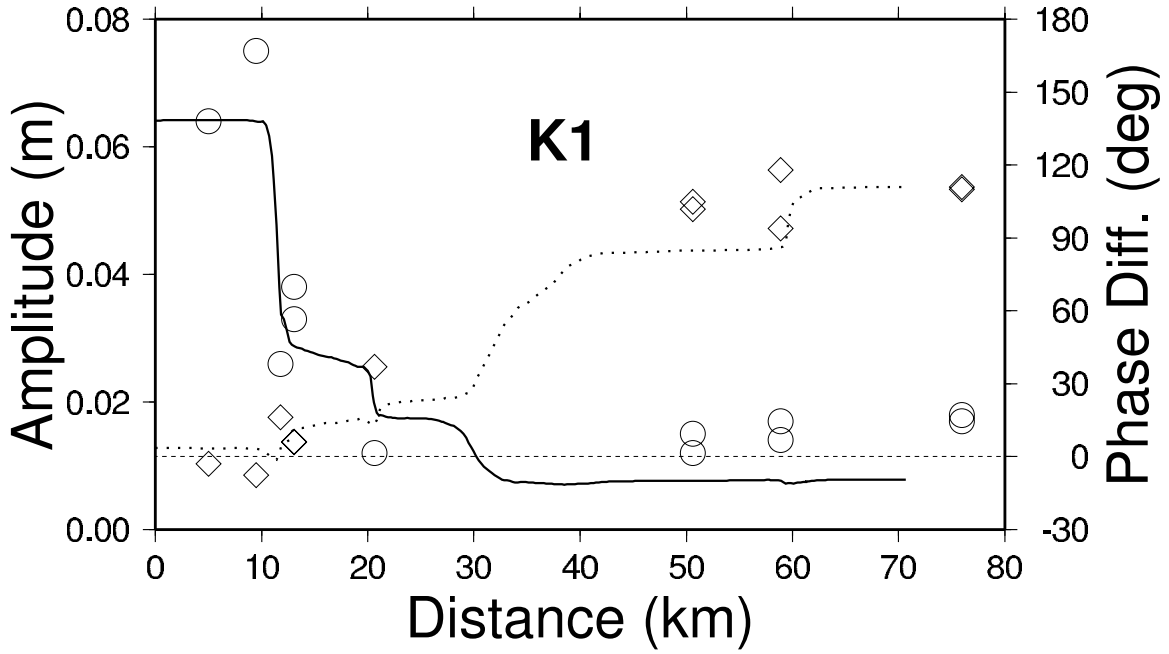

Figure 8. Amplitude (plain line) and phase (dotted line) for the K1 constituent along the line shown in Fig. 1. The observed harmonics are shown for comparison as open circles (amplitude) and open diamonds (phase). The thin dashed line shows the zero phase line.

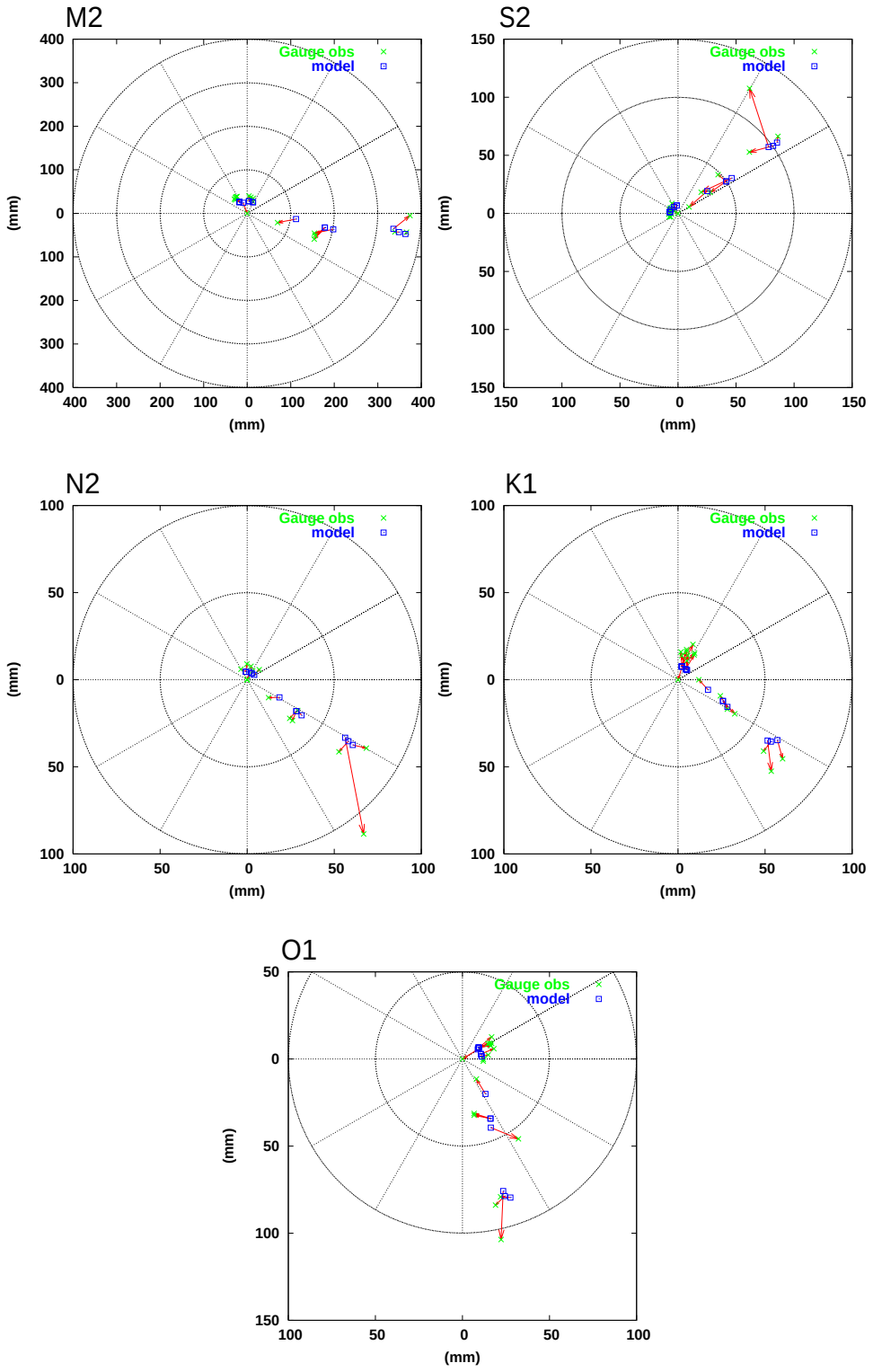

Figure 9. Polar plots for each tidal constituent showing the model solution against the observations. The amplitude is given by the radial direction and the phase by the orthoradial direction. A long arrow indicates a large discrepancy in either amplitude or phase or both.

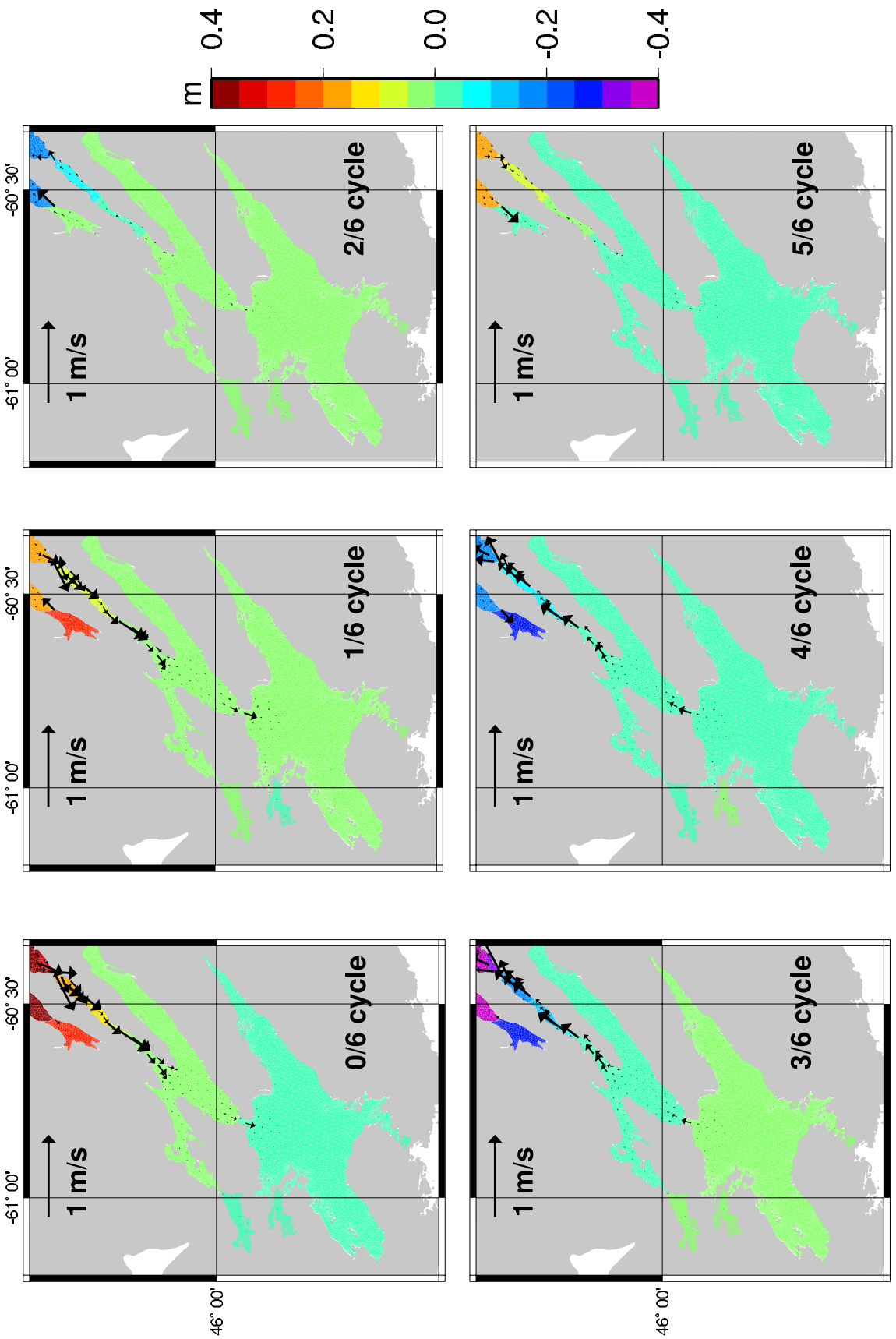

Figure 10. Elevation and currents at 6 stages of the M2 tide relative to high tide at North Sydney.

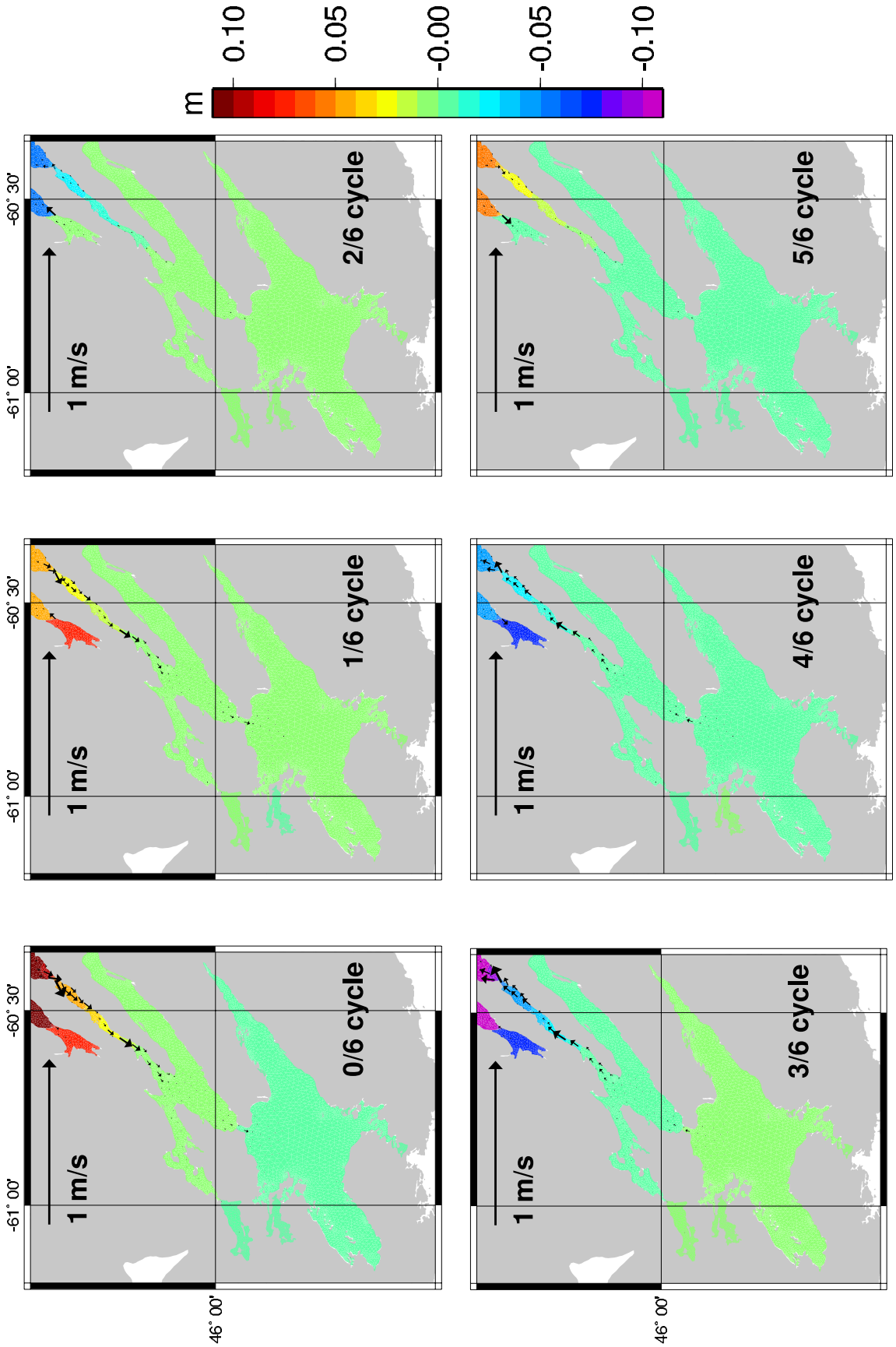

Figure 11. Elevation and currents at 6 stages of the S2 tide relative to high tide at North Sydney.

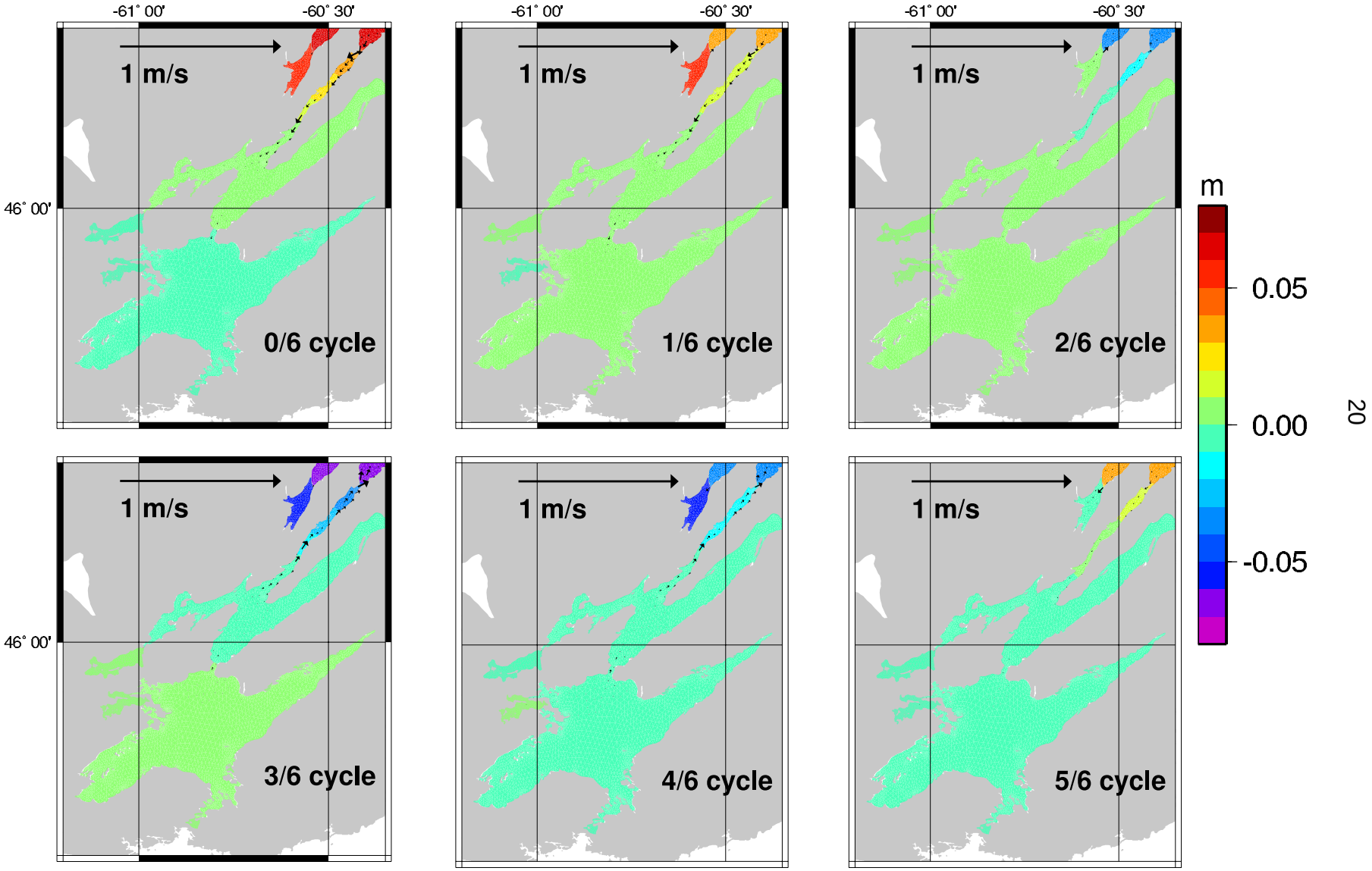

Figure 12. Elevation and currents at 6 stages of the N2 tide relative to high tide at North Sydney.

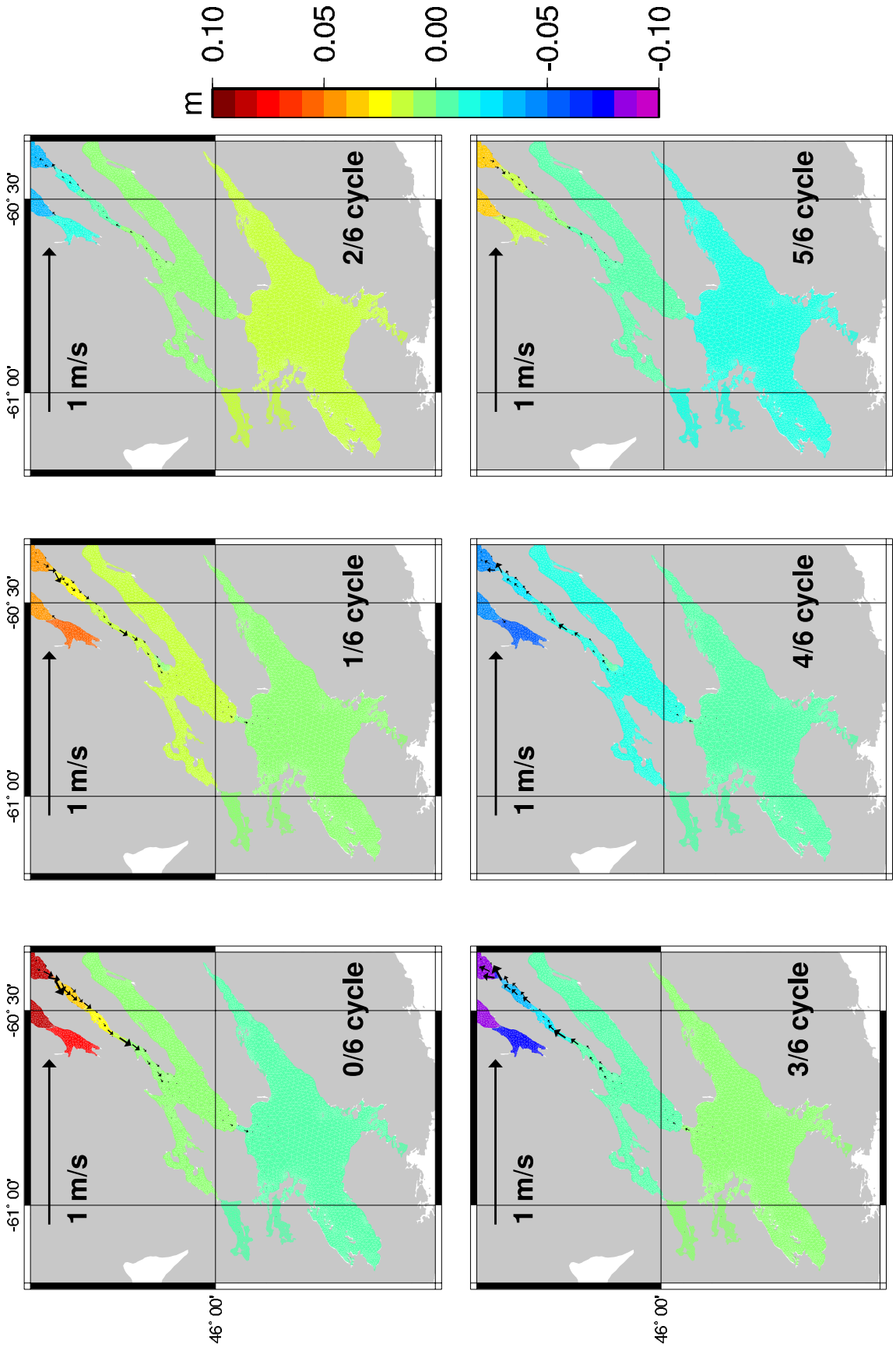

Figure 13. Elevation and currents at 6 stages of the O1 tide relative to high tide at North Sydney.

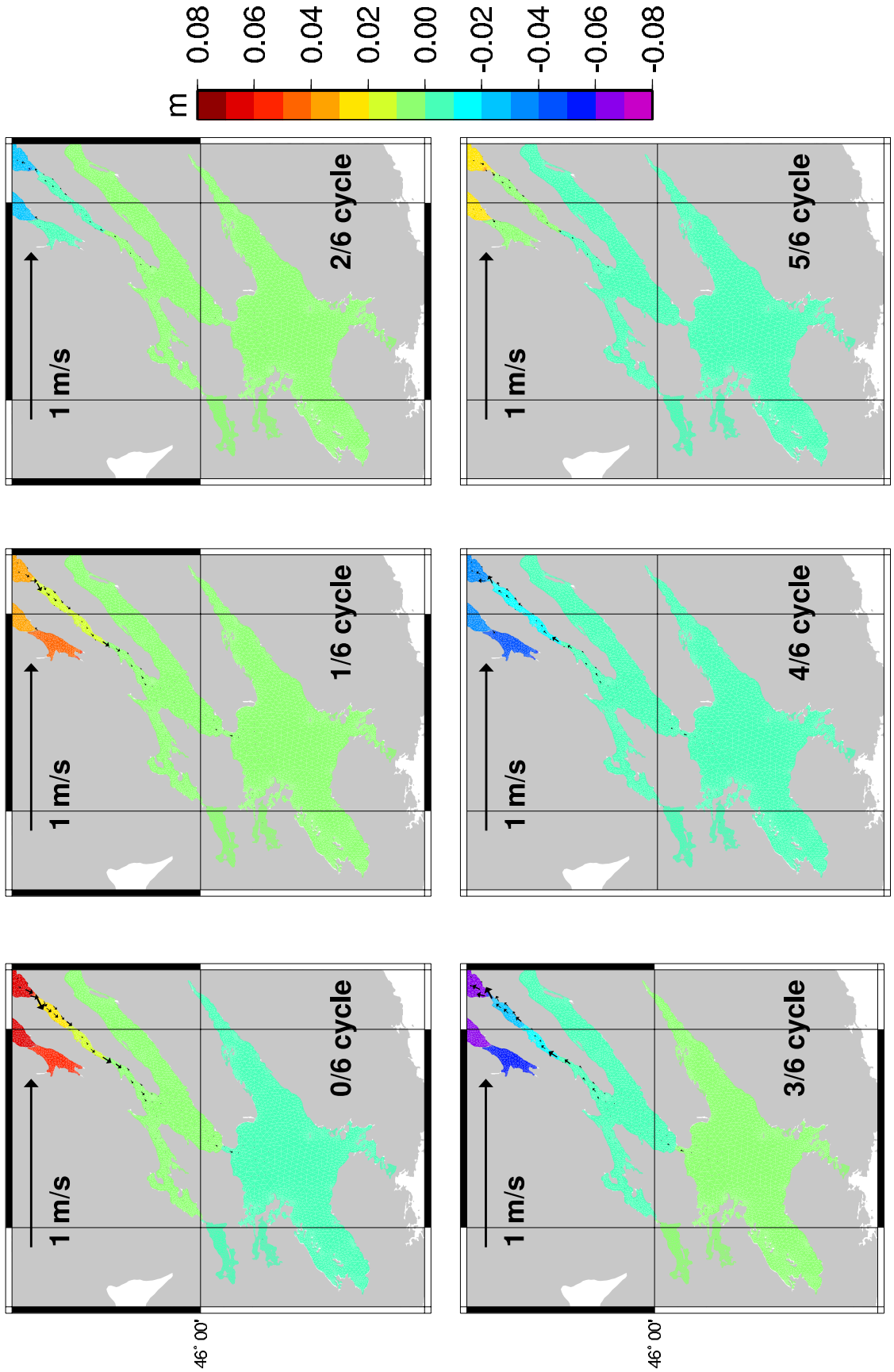

Figure 14. Elevation and currents at 6 stages of the K1 tide relative to high tide at North Sydney.

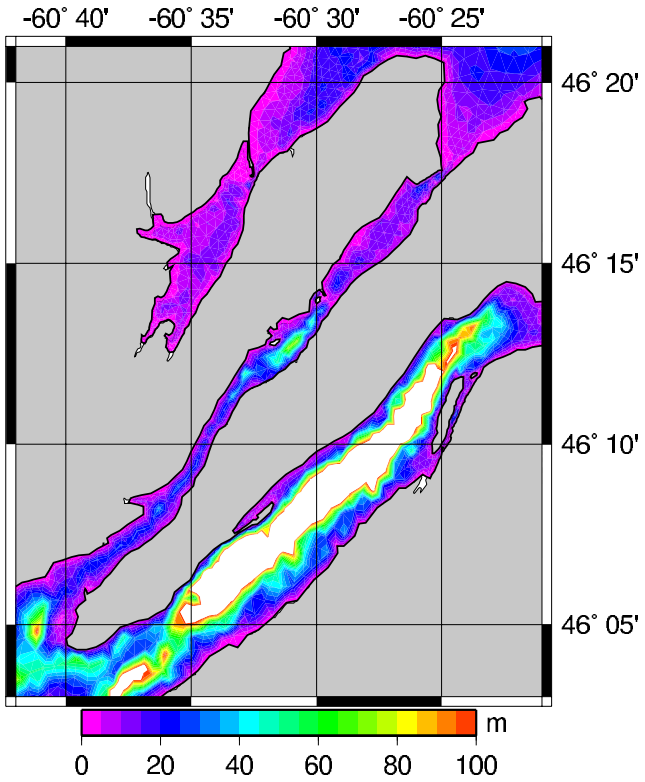

Figure 15(a). Model bathymetry of the Great Bras d'Or Channel.

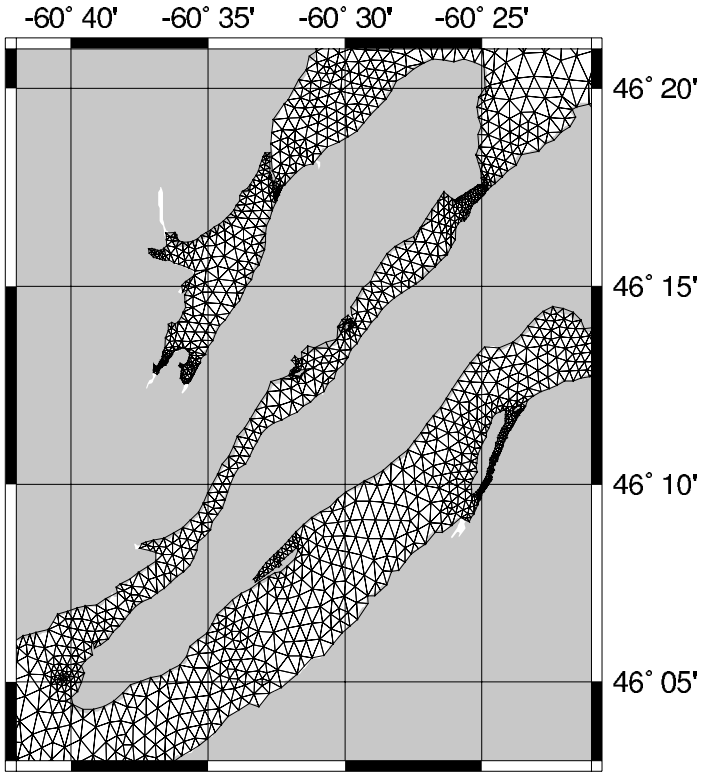

Figure 15(b) Finite element mesh for the Great Bras d'Or Channel.

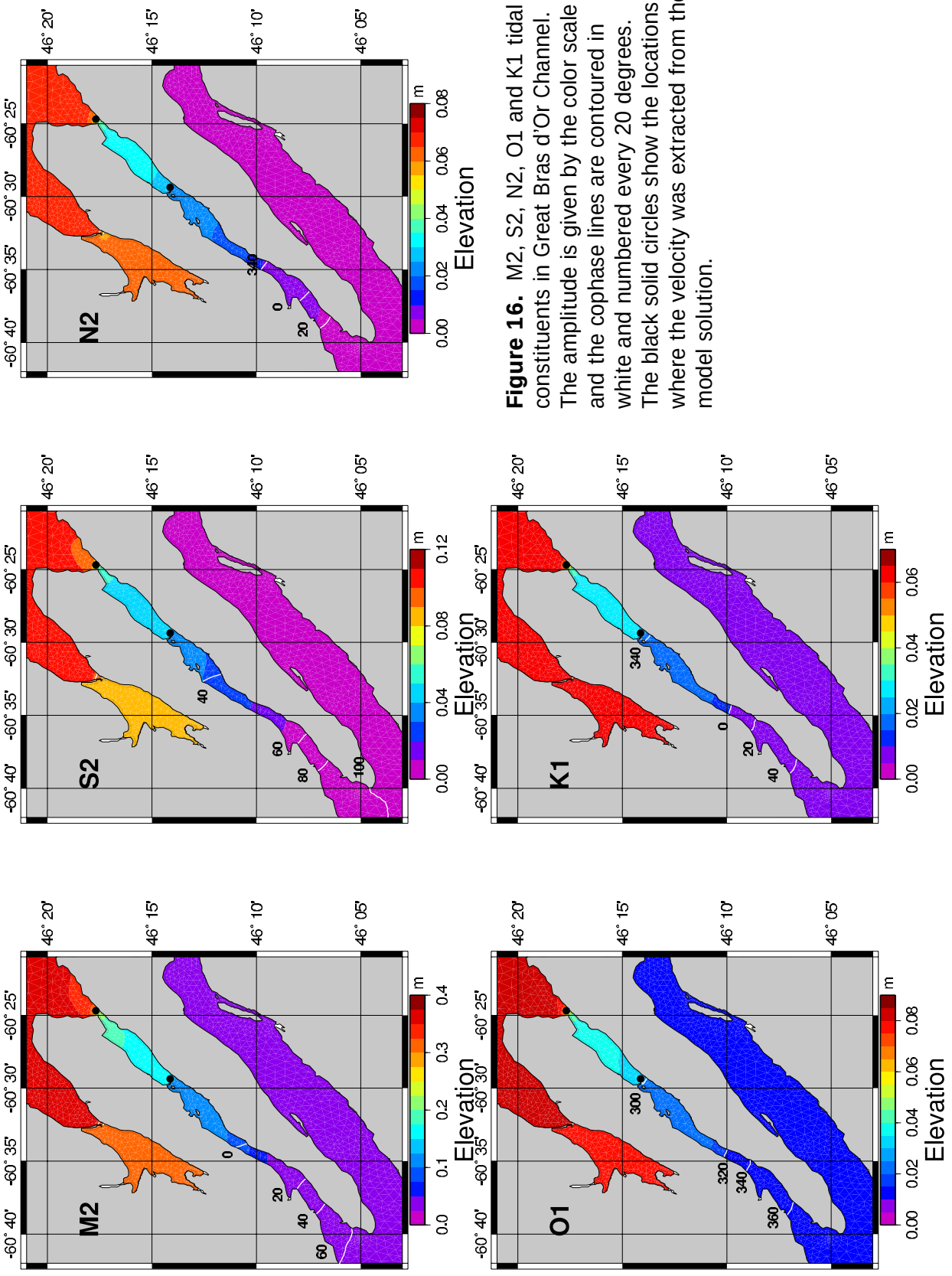

Figure 16. M2, S2, N2, O1 and K1 tidal constituents in Great Bras d'Or Channel. The amplitude is given by the color scale and the cophase lines are contoured in white and numbered every 20 degrees. The black solid circles show the locations where the velocity was extracted from the model solution.

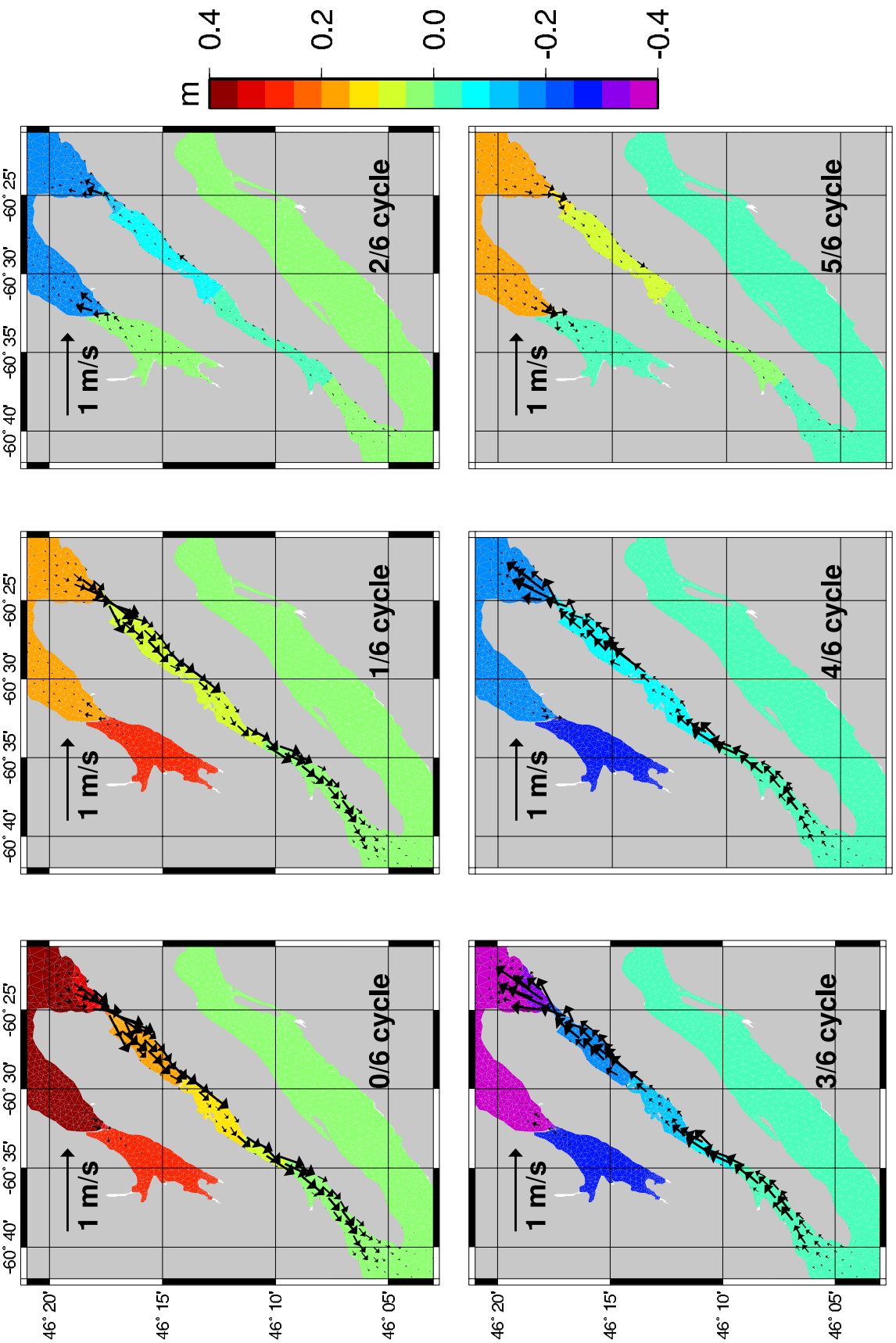

Figure 17. Elevation and currents at 6 stages of the M2 tidal cycle relative to high tide at North Sydney.

.

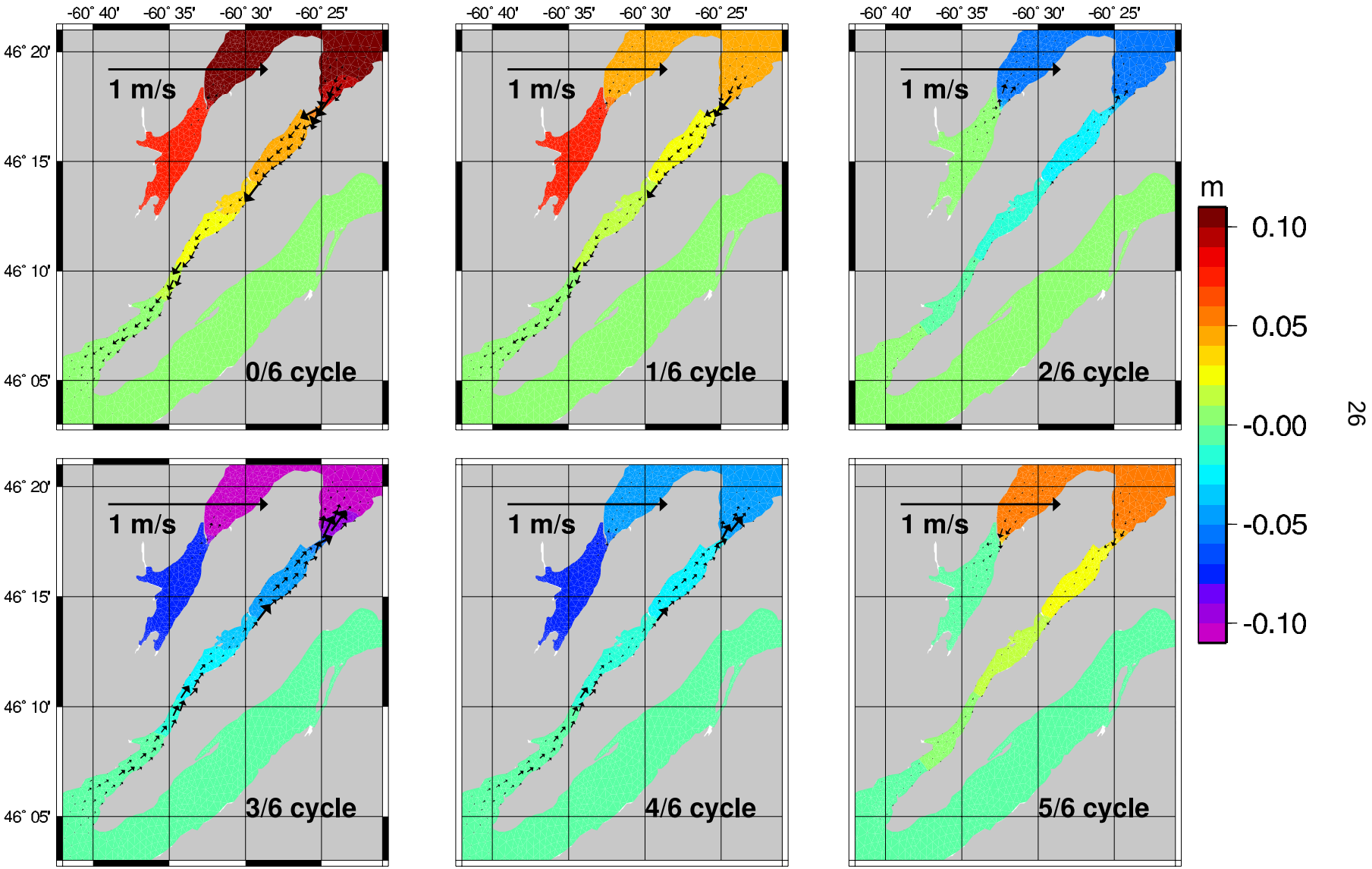

Figure 18. Elevation and currents at 6 stages of the S2 tidal cycle relative to high tide at North Sydney.

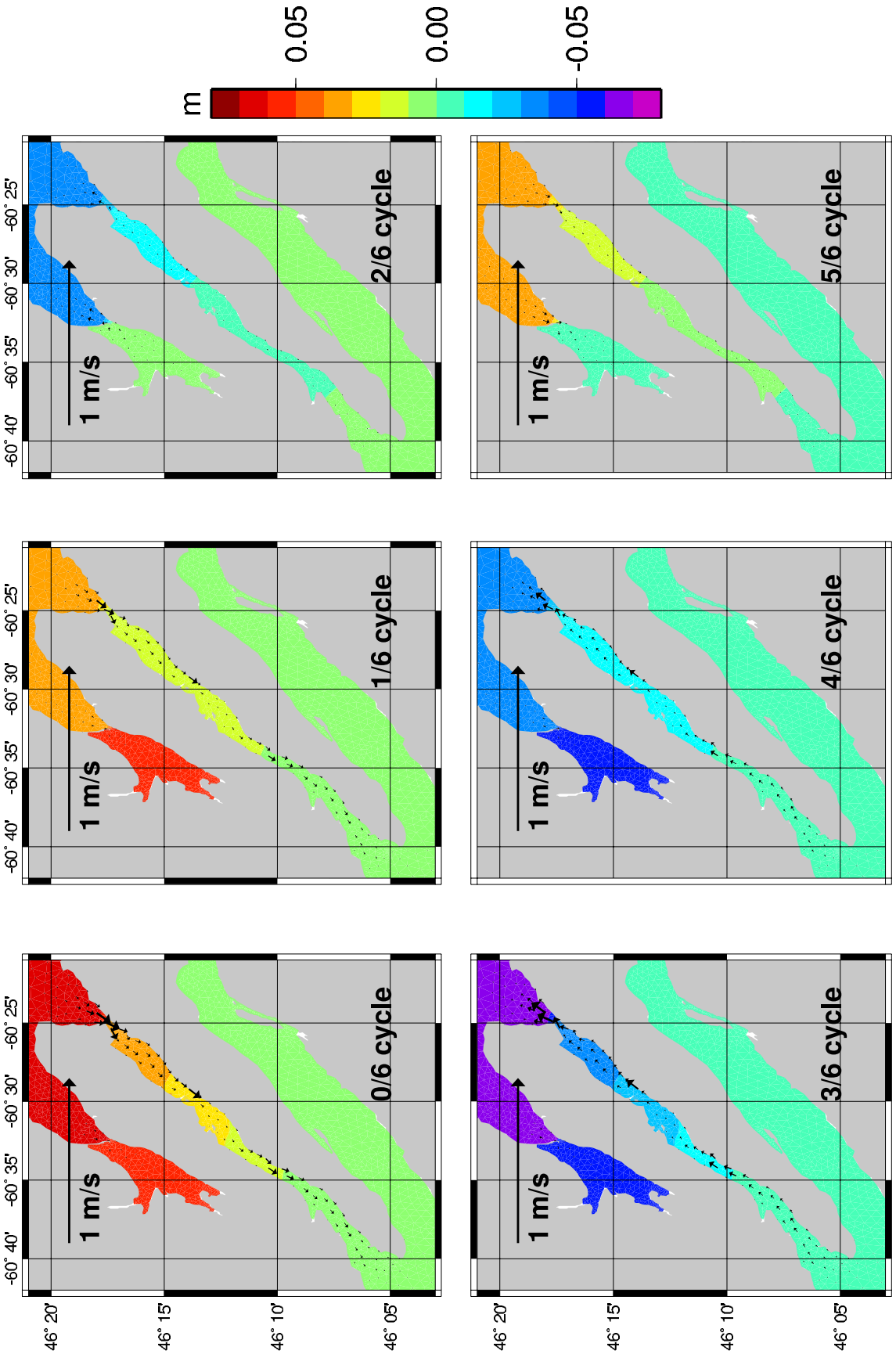

Figure 19. Elevation and currents at 6 stages of the N2 tidal cycle relative to high tide at North Sydney.

.

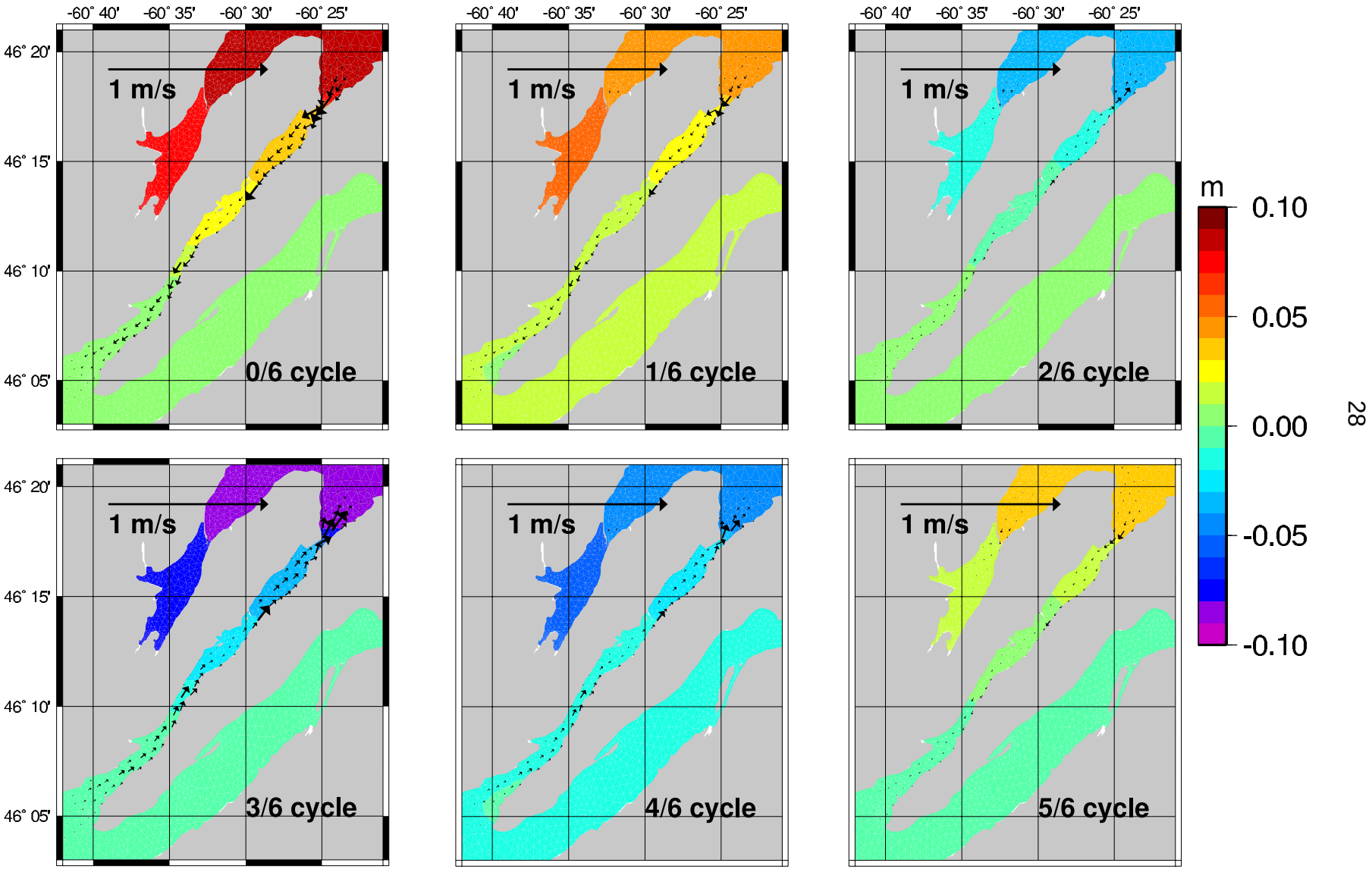

Figure 20. Elevation and currents at 6 stages of the O1 tidal cycle relative to high tide at North Sydney.

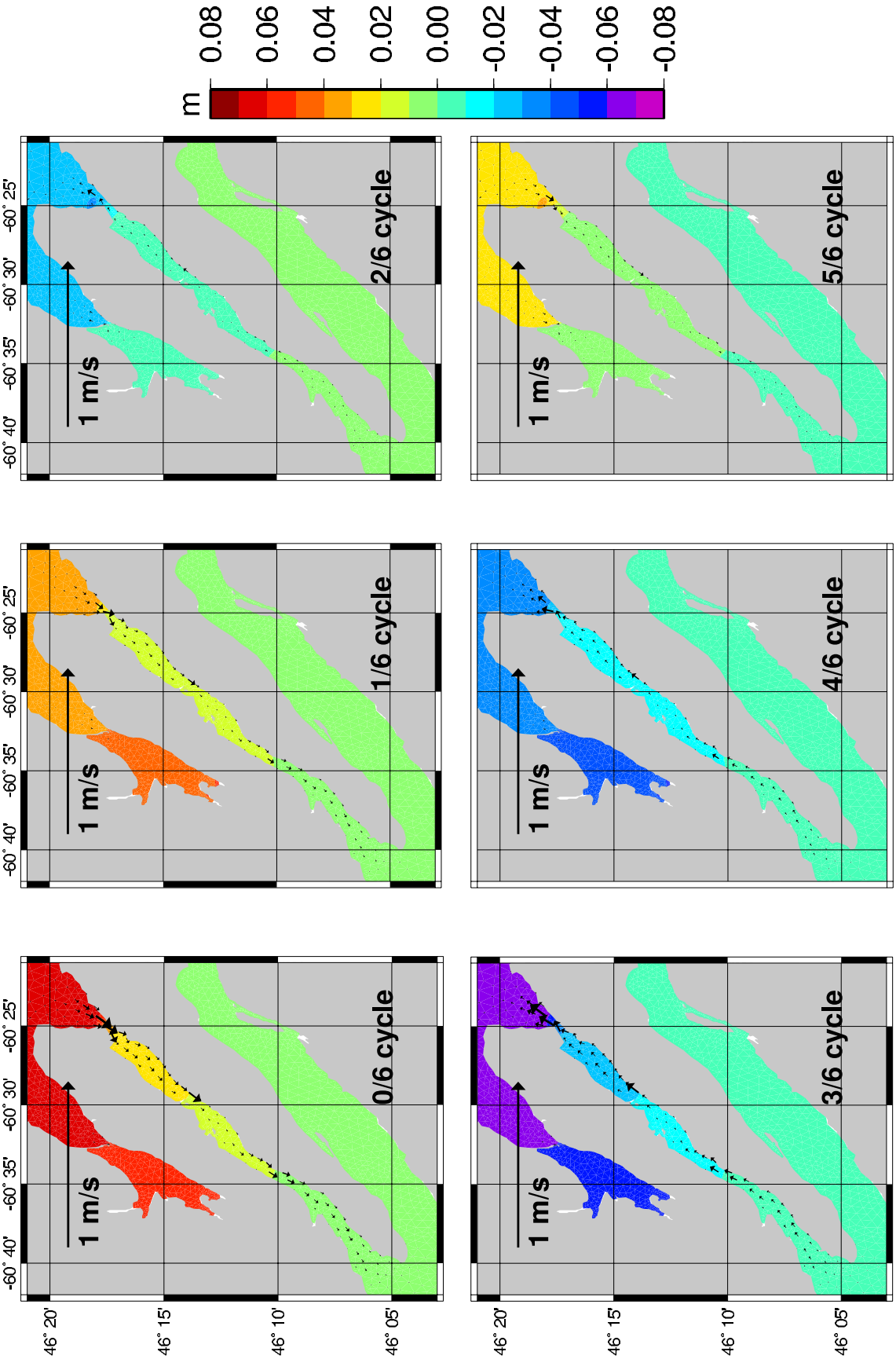

Figure 21. Elevation and currents at 6 stages of the K1 tidal cycle relative to high tide at North Sydney.

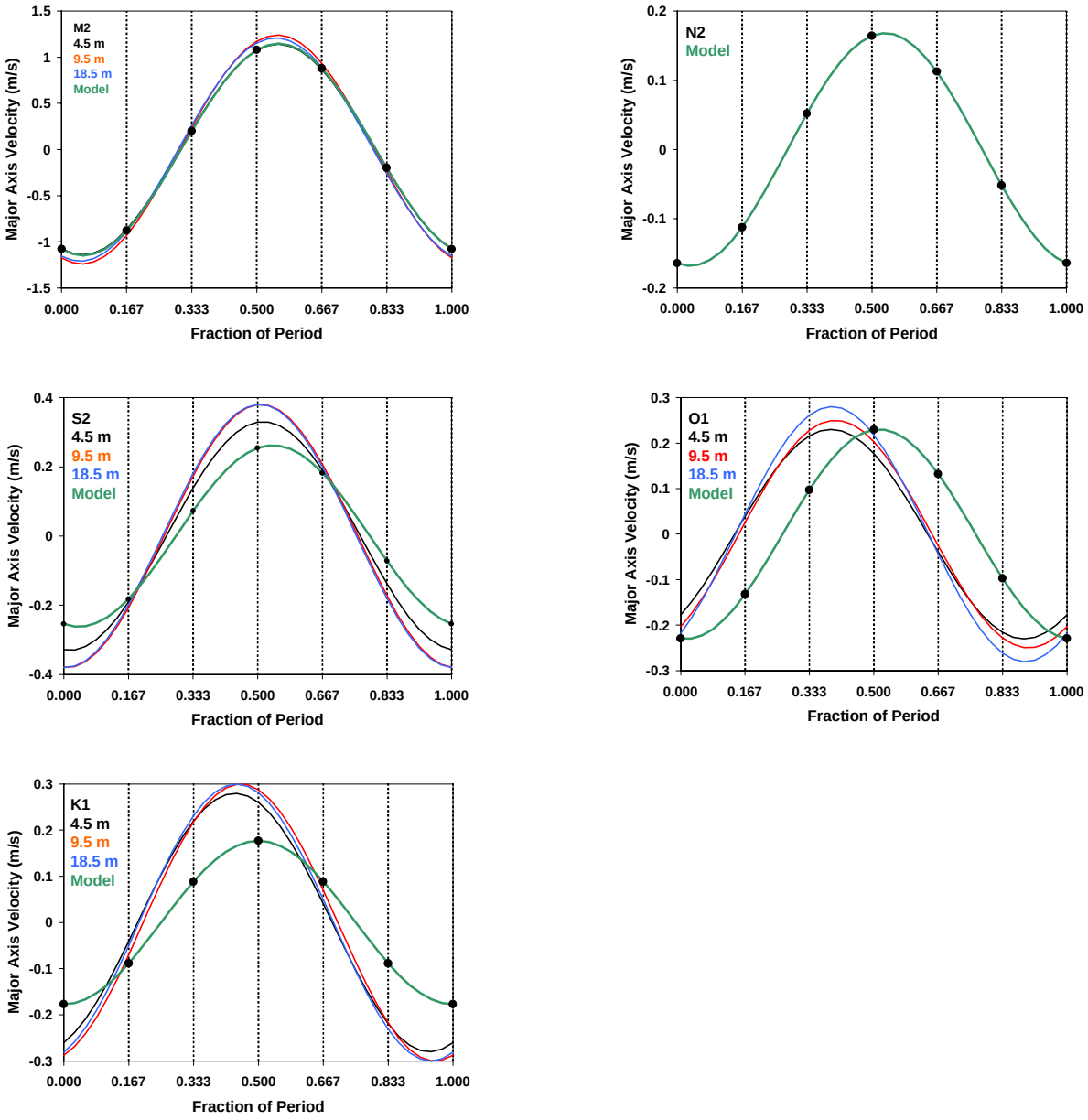

Figure 22. Velocity along the major axis close Carey Pt. in Great Bras d'Or Channel oriented offshore for the five major tidal constituents. For each constituent, a full tidal cycle has been plotted. The velocities are relative to high tide at North Sydney which occurs at 0 fraction of the tidal period. The dots indicate the phase of the tide at which Fig. 17-21 are plotted. The major axis tidal currents from an ADCP mooring near Carey Point are also shown.

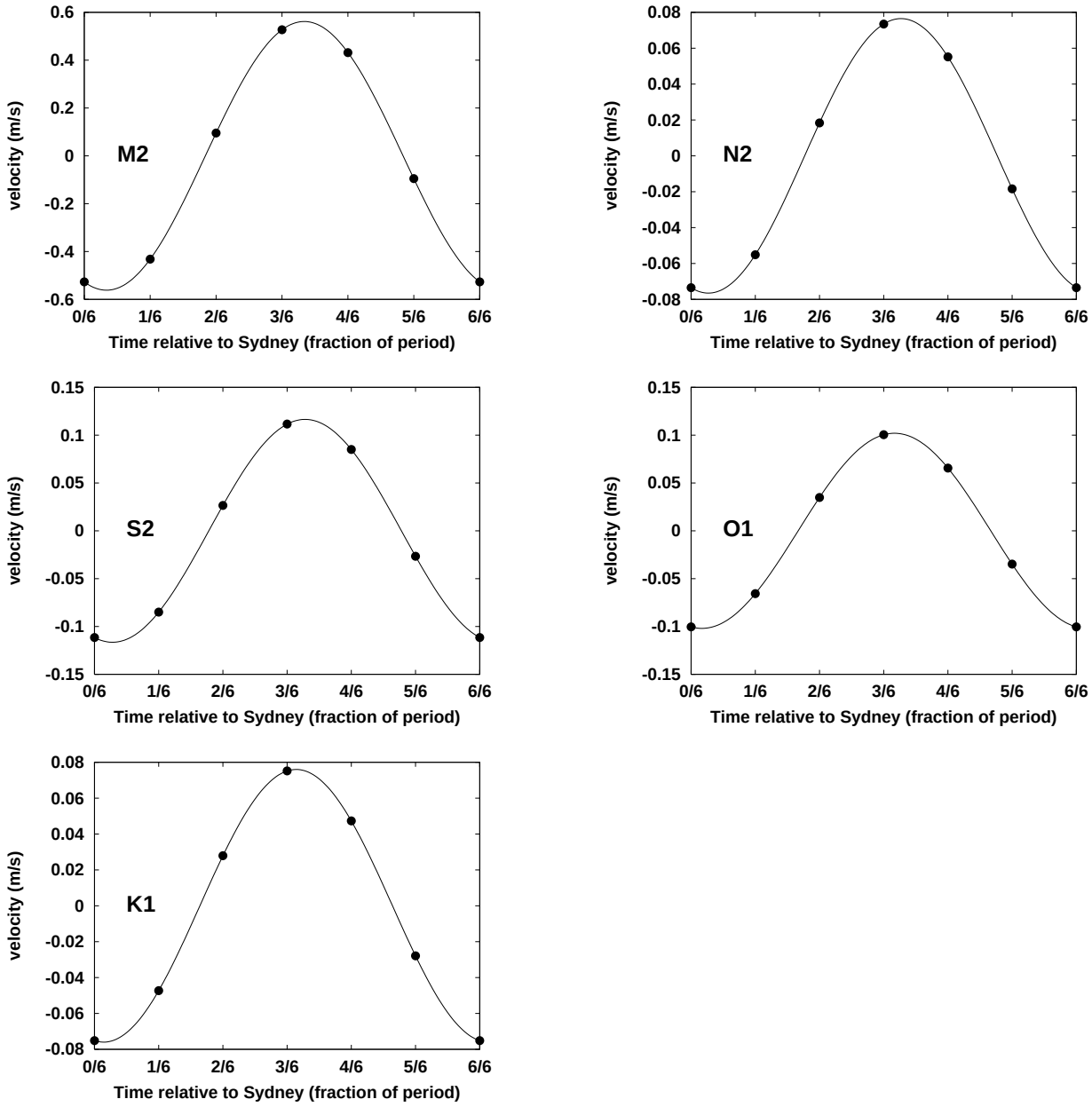

Figure 23. Velocity amplitude underneath the bridge at Seal Island in Great Bras d'Or Channel oriented offshore for five tidal constituents. The phase is relative to high tide at North Sydney. The dots indicate the phase of the tide at which Fig. 17-21 are plotted.

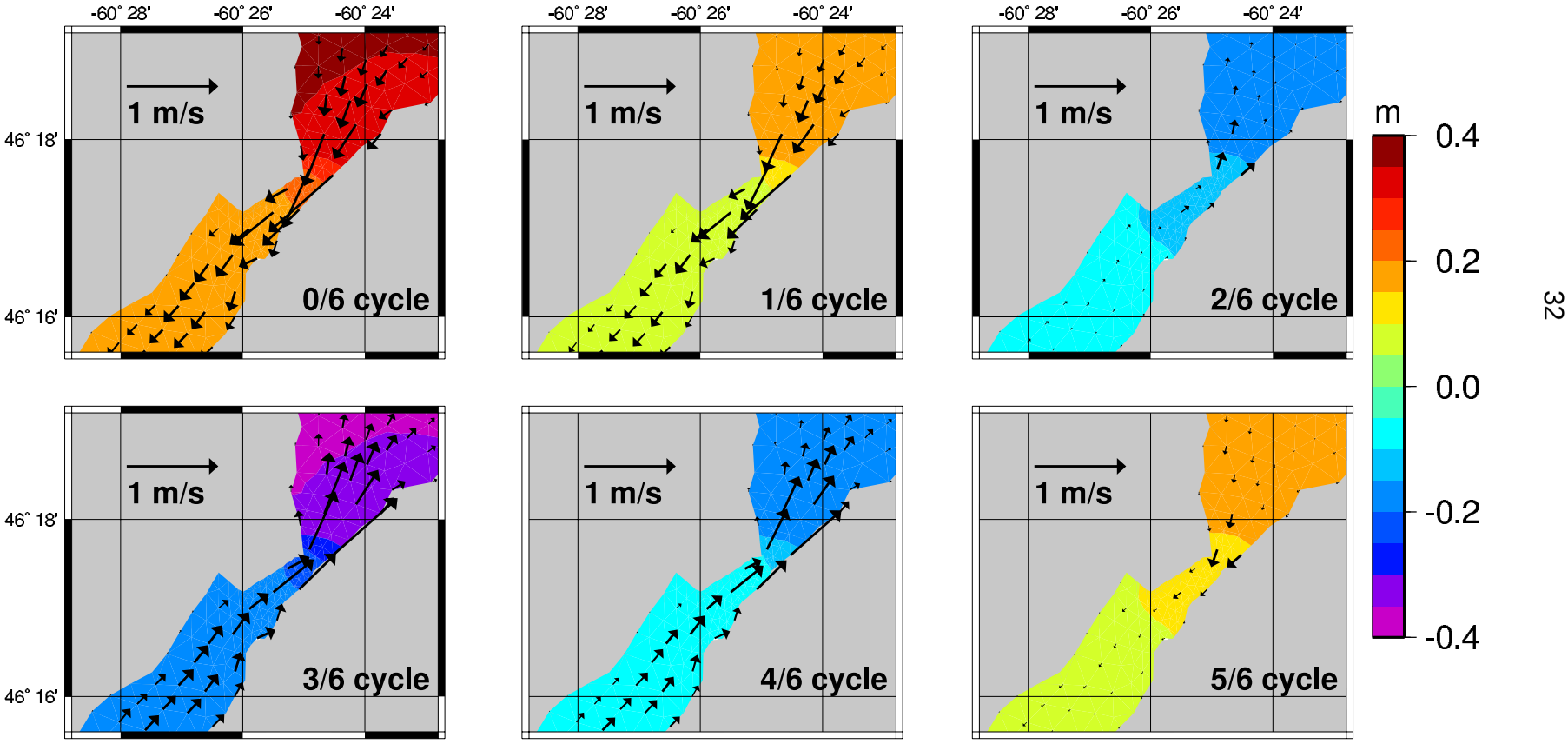

Figure 24. Elevation and currents at 6 stages of the M2 tidal cycle relative to high tide at North Sydney.

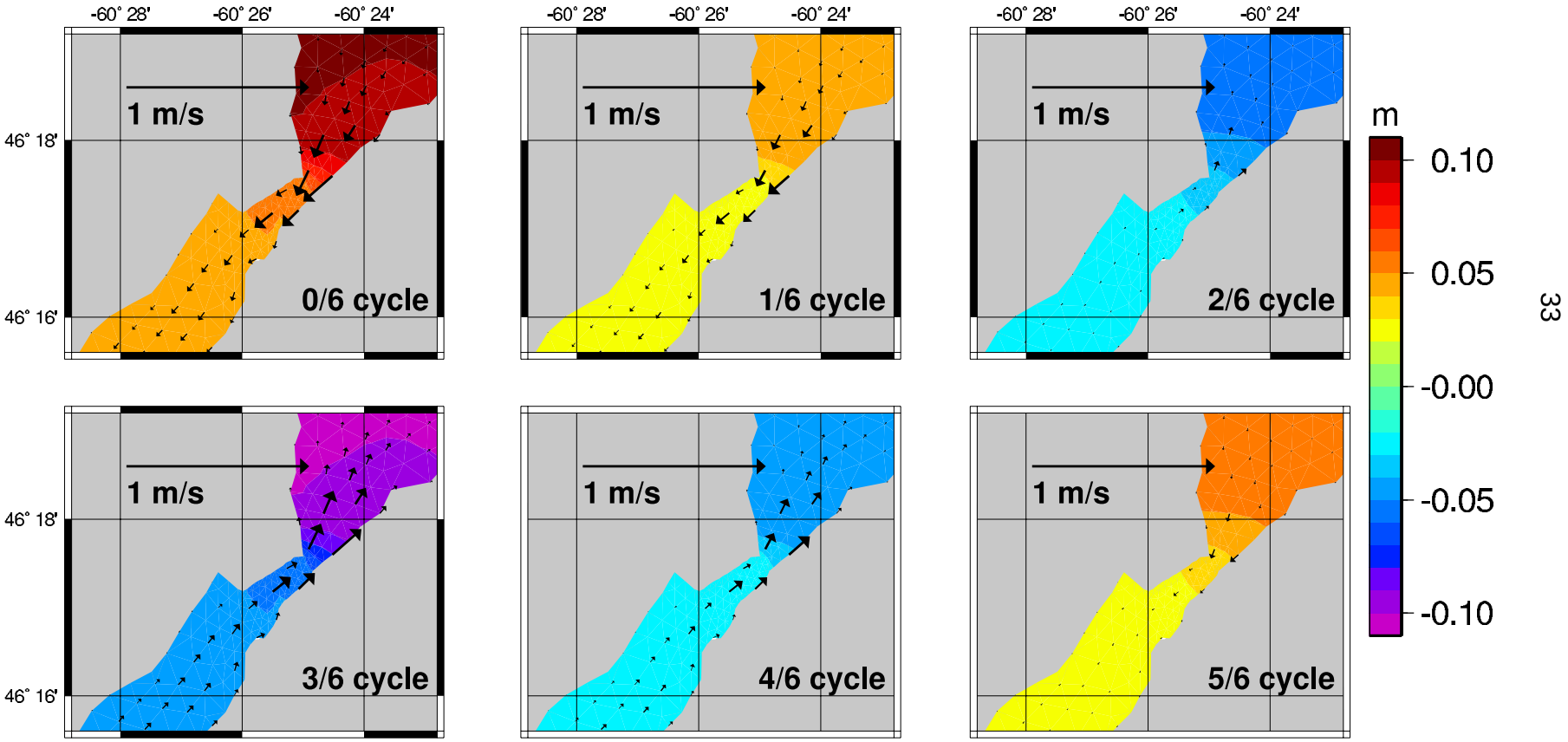

Figure 25. Elevation and currents at 6 stages of the S2 tidal cycle relative to high tide at North Sydney.

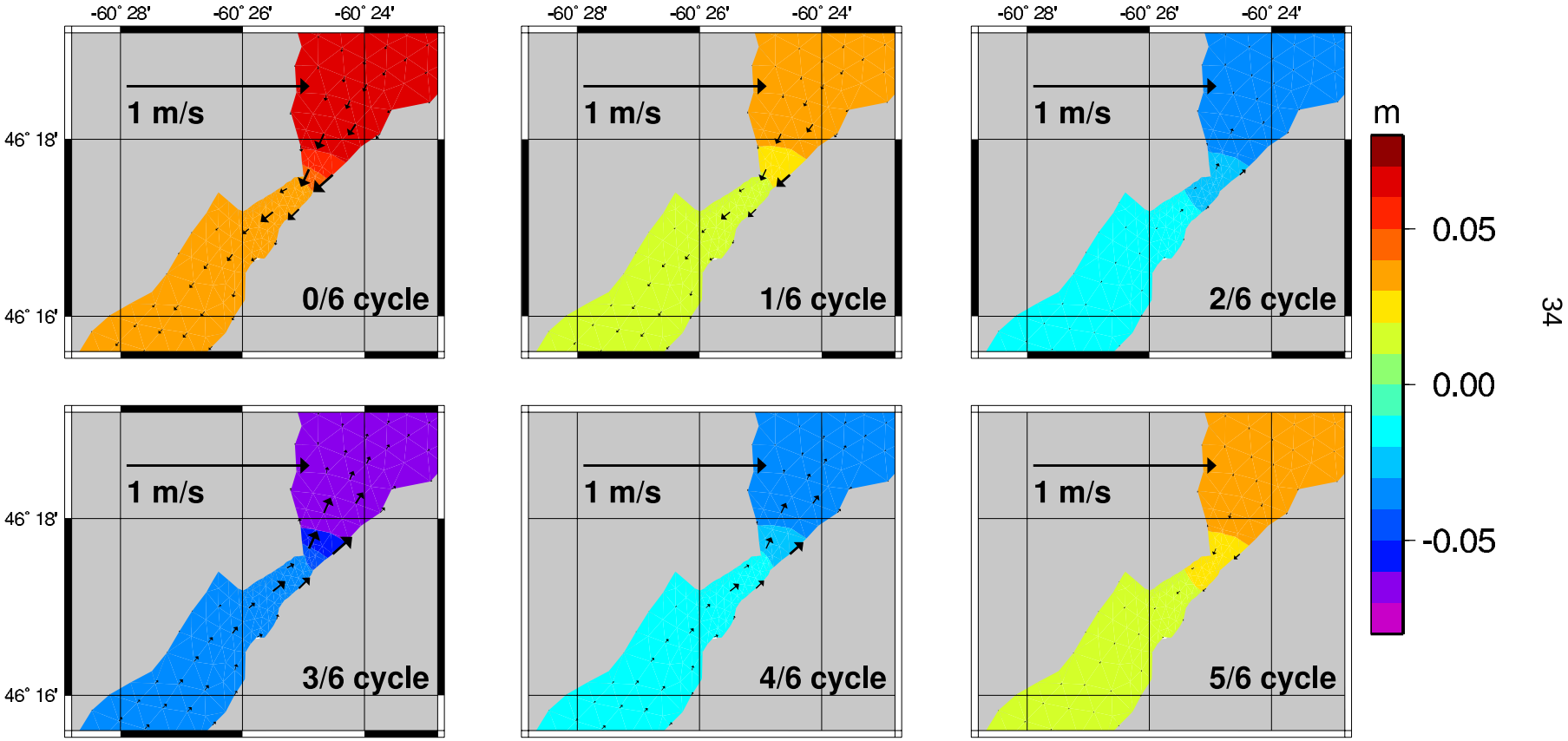

Figure 26. Elevation and currents at 6 stages of the N2 tidal cycle relative to high tide at North Sydney.

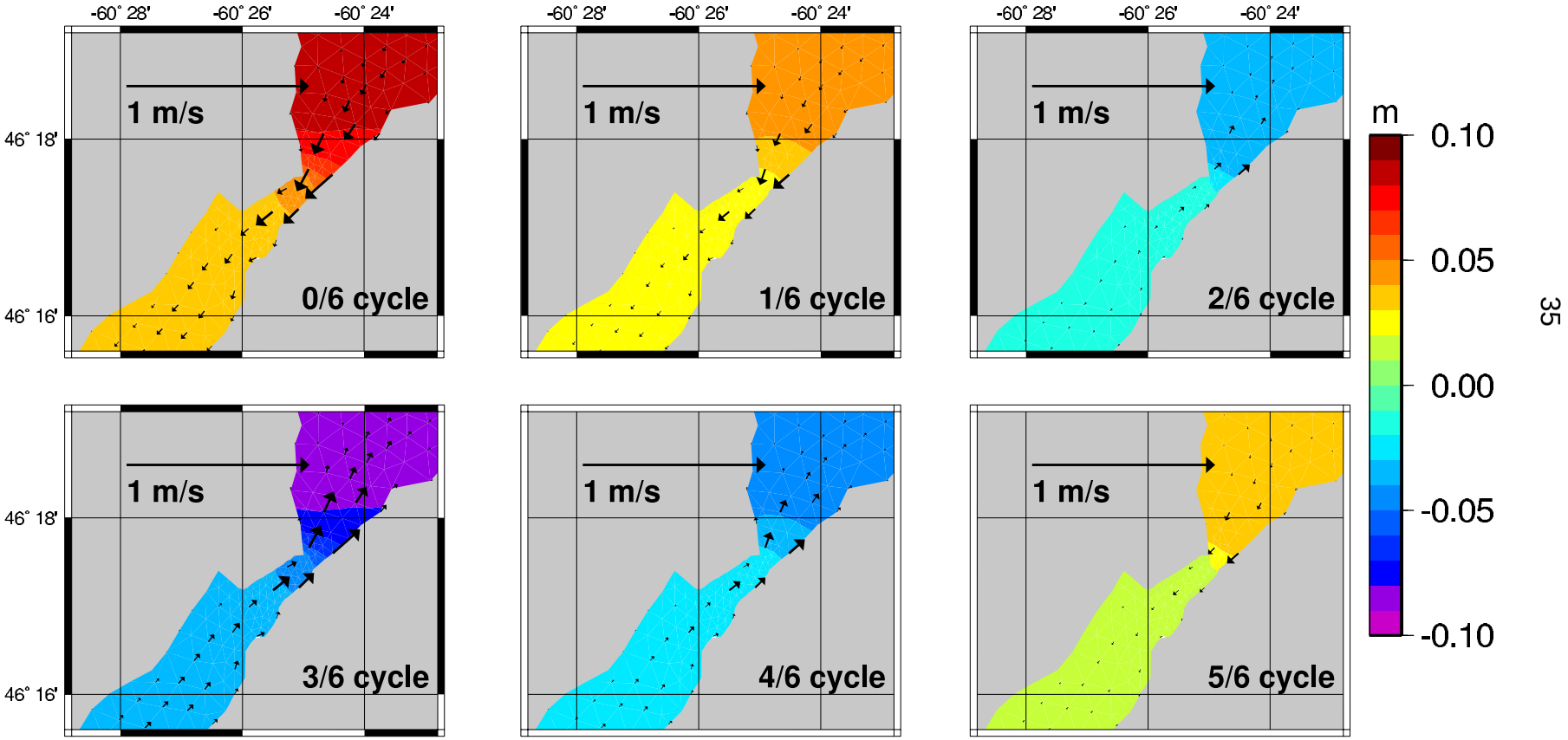

Figure 27. Elevation and currents at 6 stages of the O1 tidal cycle relative to high tide at North Sydney.

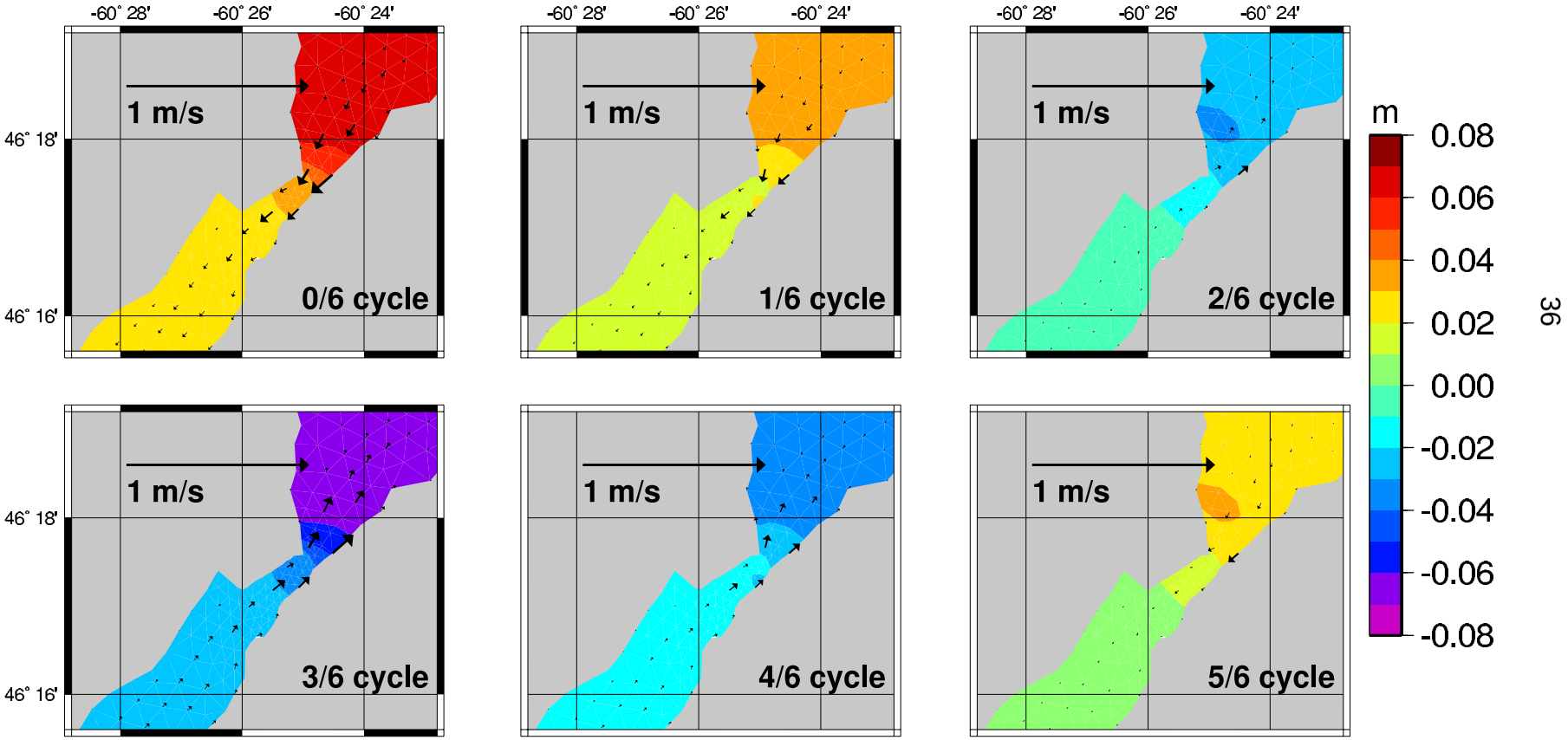

Figure 28. Elevation and currents at 6 stages of the K1 tidal cycle relative to high tide at North Sydney.

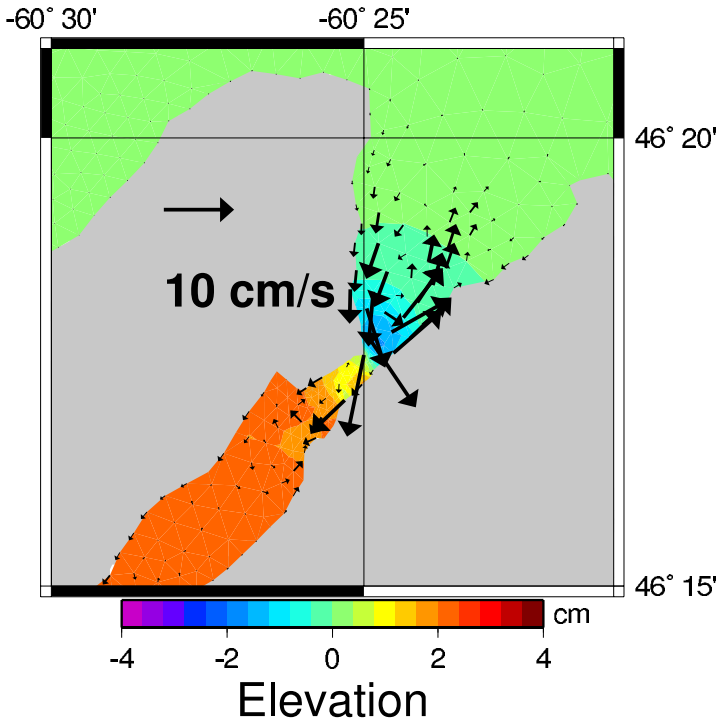

Figure 29(a). Residual elevation and currents at the entrance of Great Bras d'Or Channel. Note that the residual current was determined by averaging at each grid point for the entire 36 d run. All grid points are not plotted.

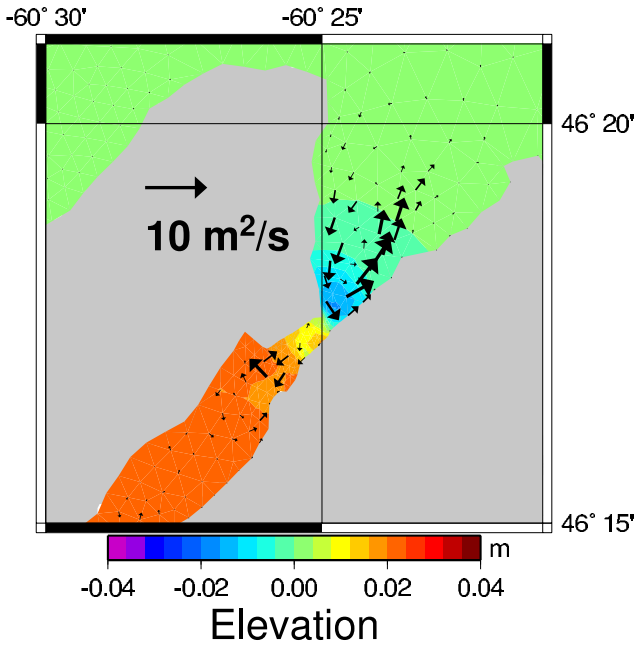

Figure 29(b). Residual elevation and residual current times depth at the entrance of Great Bras d'Or Channel. All grid points are not plotted.

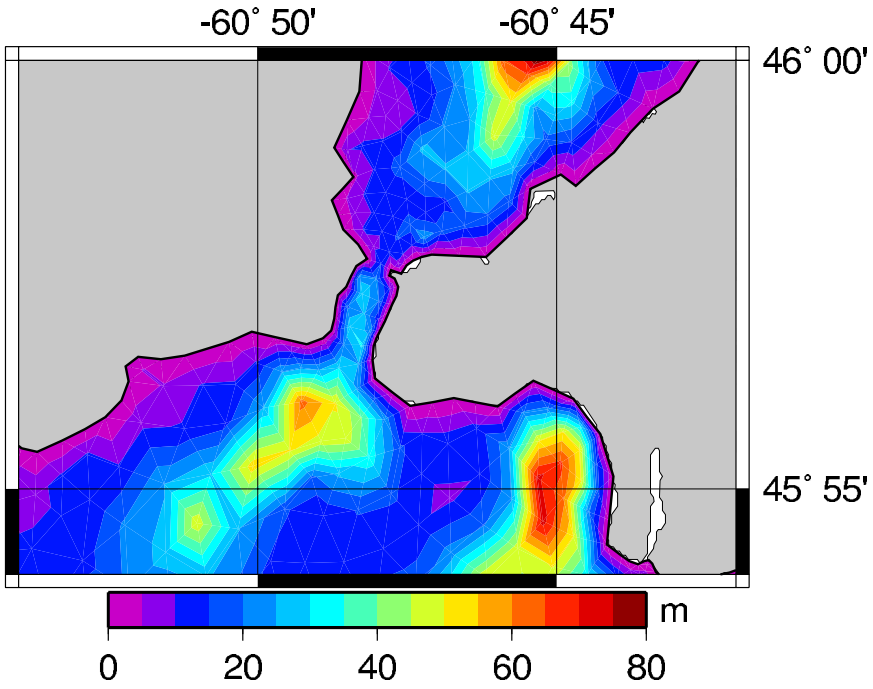

Figure 30(a). Model bathymetry in the Barra Strait region.

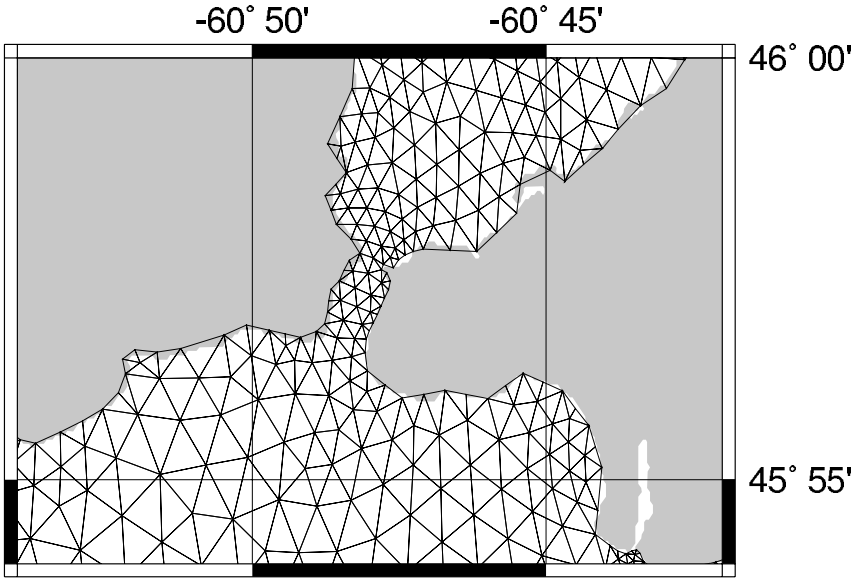

Figure 30(b). Finite element mesh for Barra Strait.

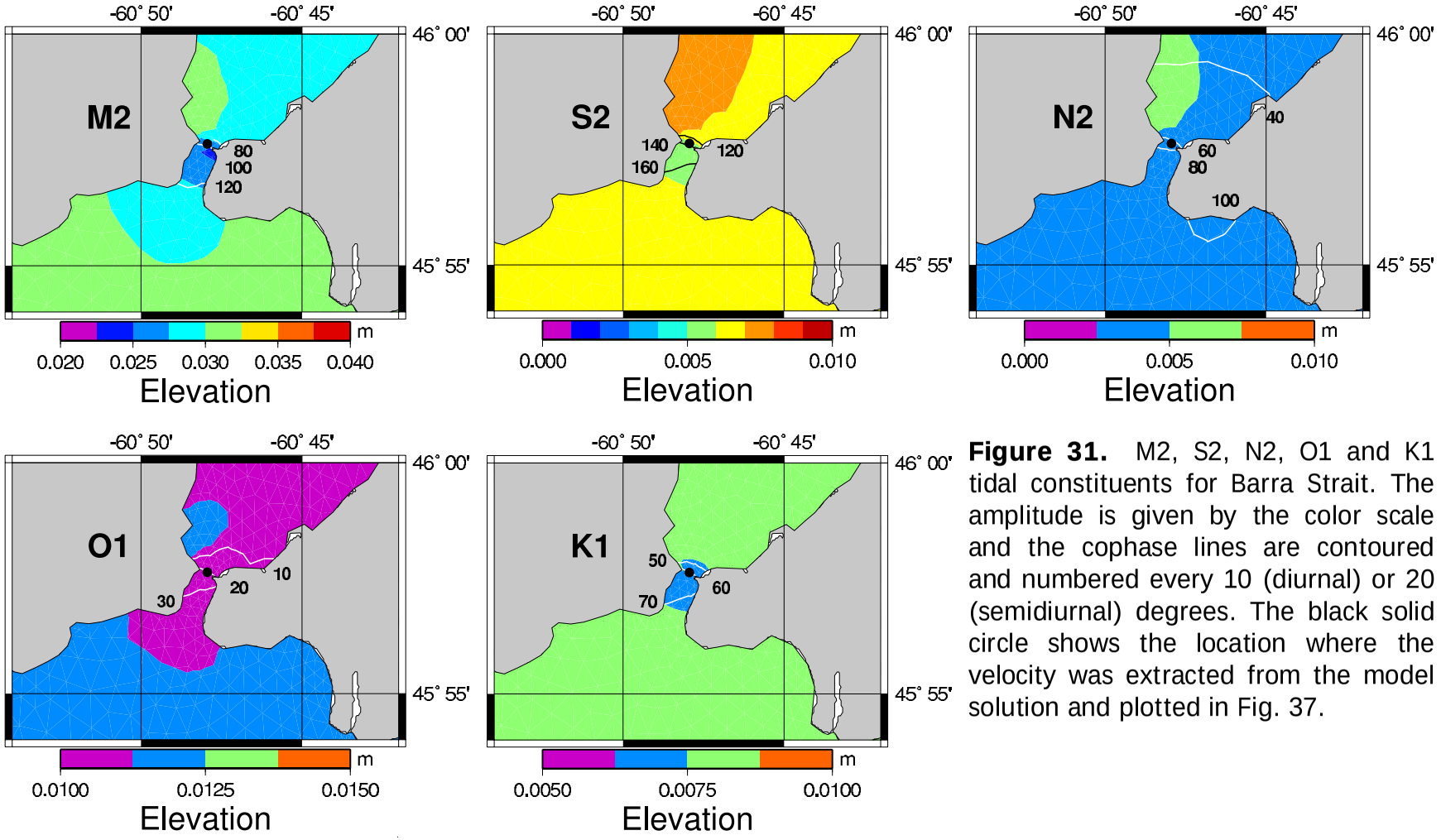

Figure 31. M2, S2, N2, O1 and K1 tidal constituents for Barra Strait. The amplitude is given by the color scale and the cophase lines are contoured and numbered every 10 (diurnal) or 20 (semidiurnal) degrees. The black solid circle shows the location where the velocity was extracted from the model solution and plotted in Fig. 37.

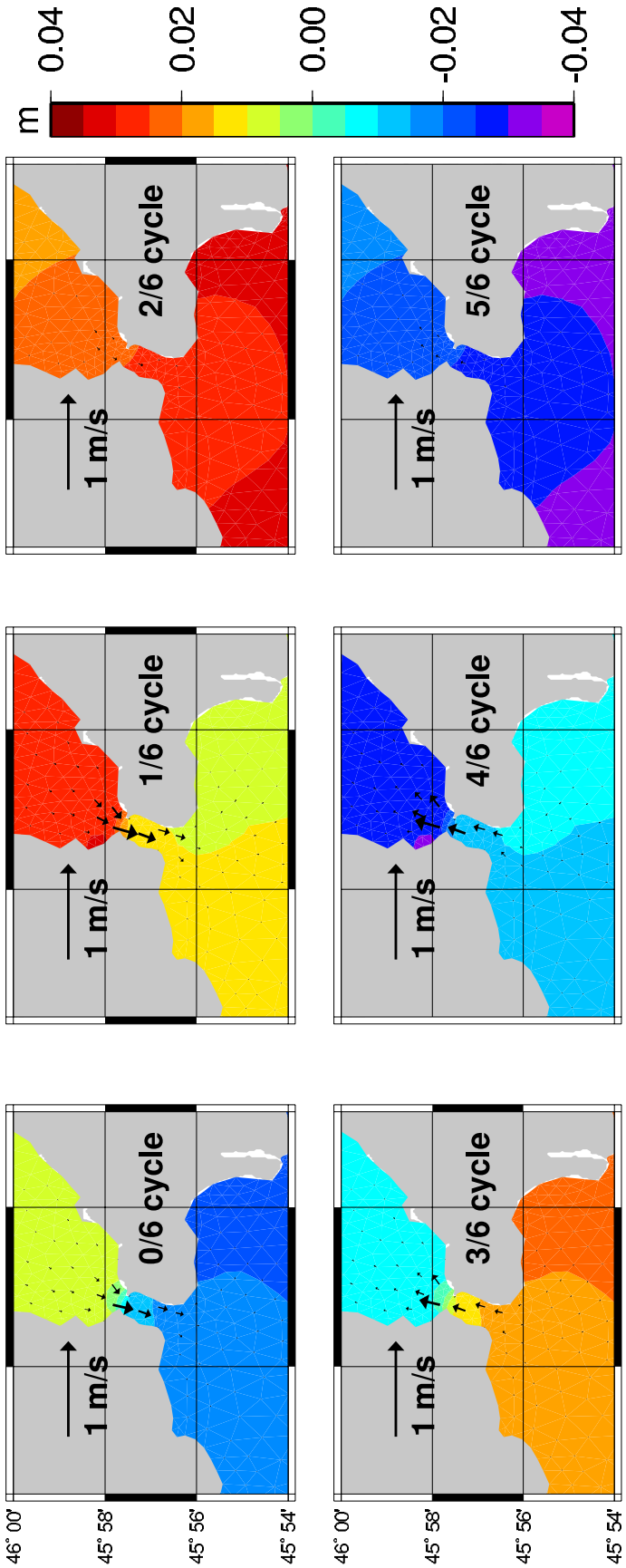

Figure 32. Elevation and currents at 6 stages of the M2 tidal cycle relative to high tide at North Sydney.

.

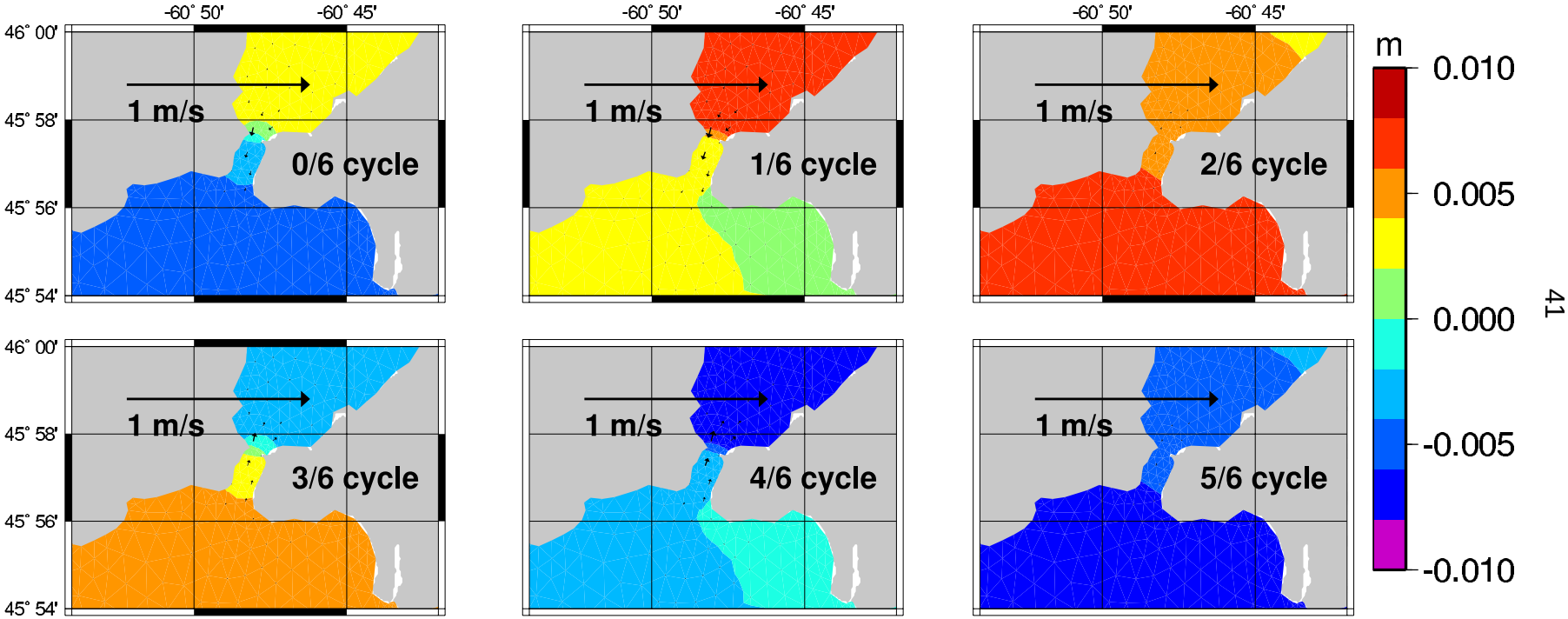

Figure 33. Elevation and currents at 6 stages of the S2 tidal cycle relative to high tide at North Sydney.

.

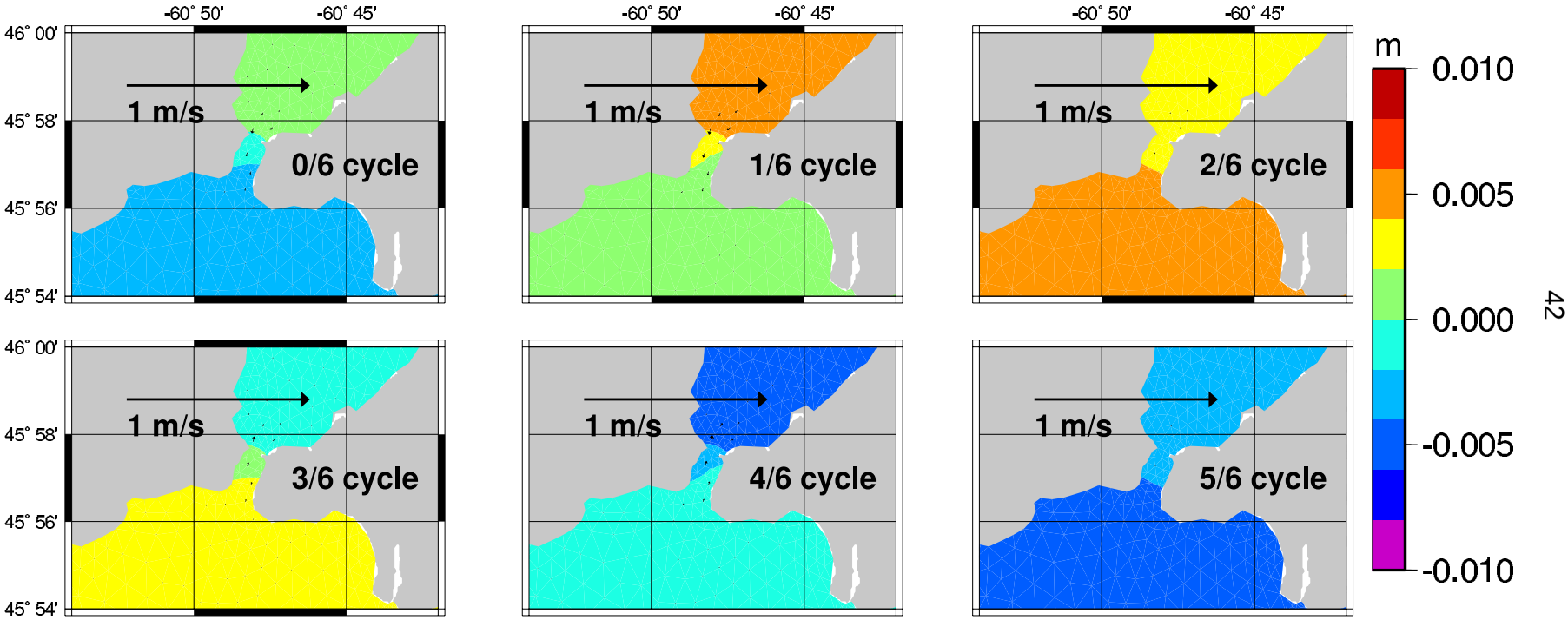

Figure 34. Elevation and currents at 6 stages of the N2 tidal cycle relative to high tide at North Sydney.

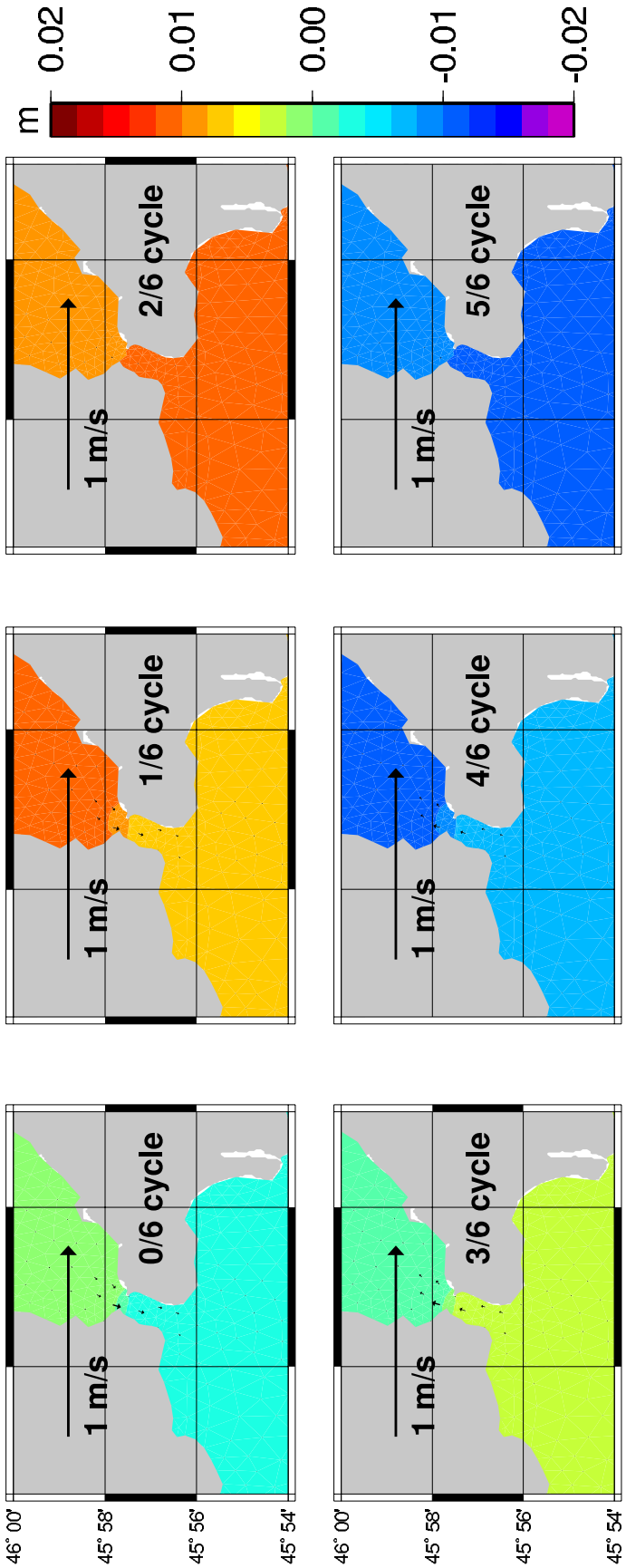

Figure 35. Elevation and currents at 6 stages of the O1 tidal cycle relative to high tide at North Sydney.

.

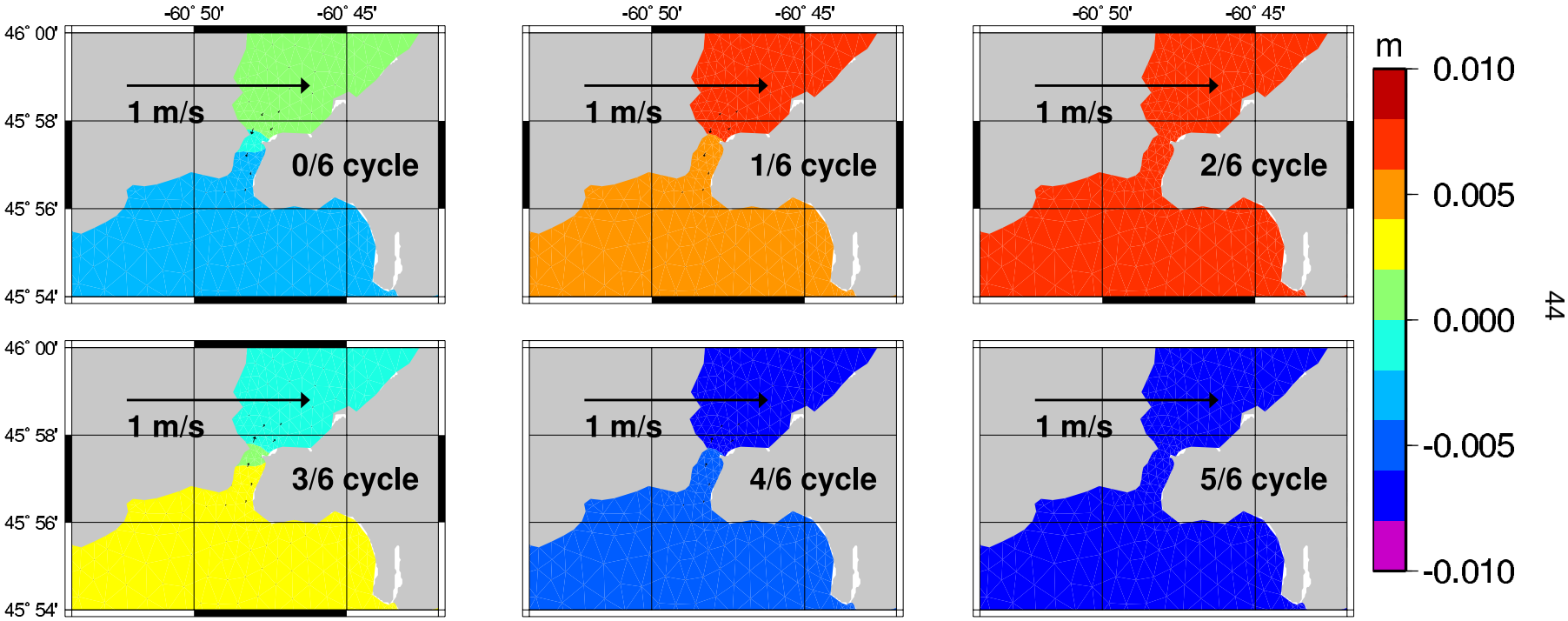

Figure 36. Elevation and currents at 6 stages of the K1 tidal cycle relative to high tide at North Sydney.

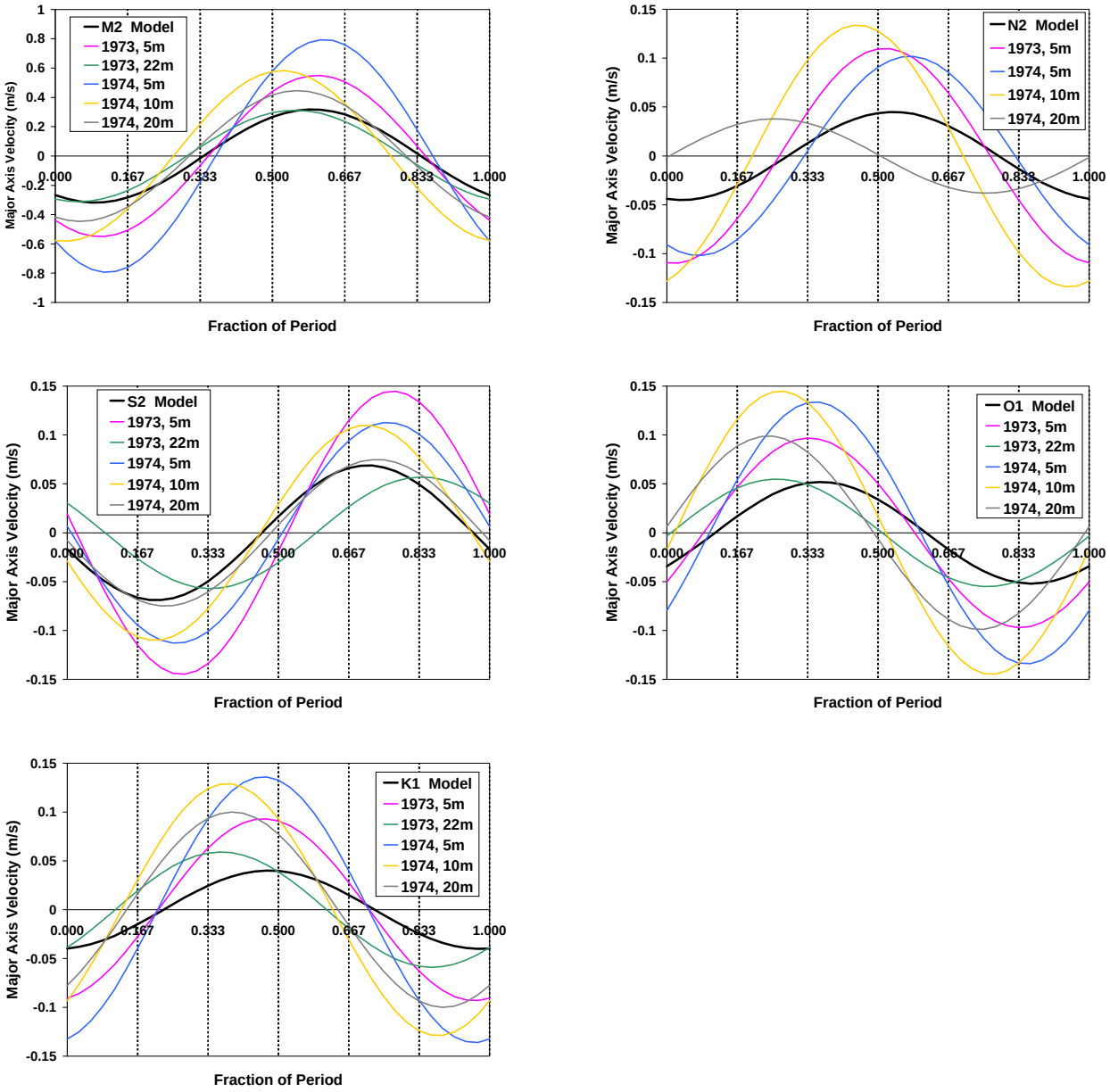

Figure 37. Tidal currents along major axis along Barra Strait oriented offshore for five tidal constituents. The phase is relative to high tide at North Sydney. The major axis tidal currents from 2 current meter moorings in Barra Strait are also shown.

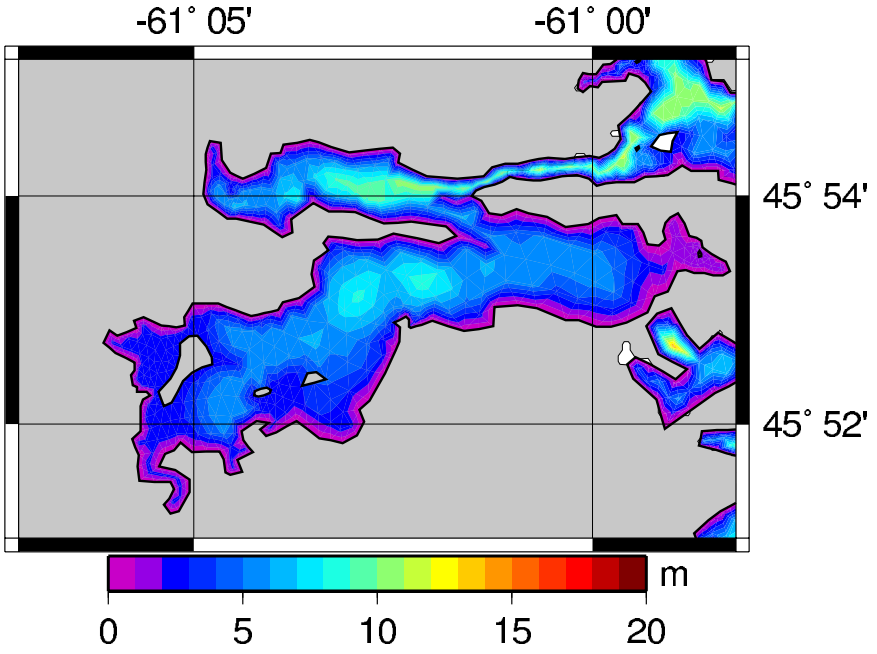

Figure 38(a). Model bathymetry for Denys Basin.

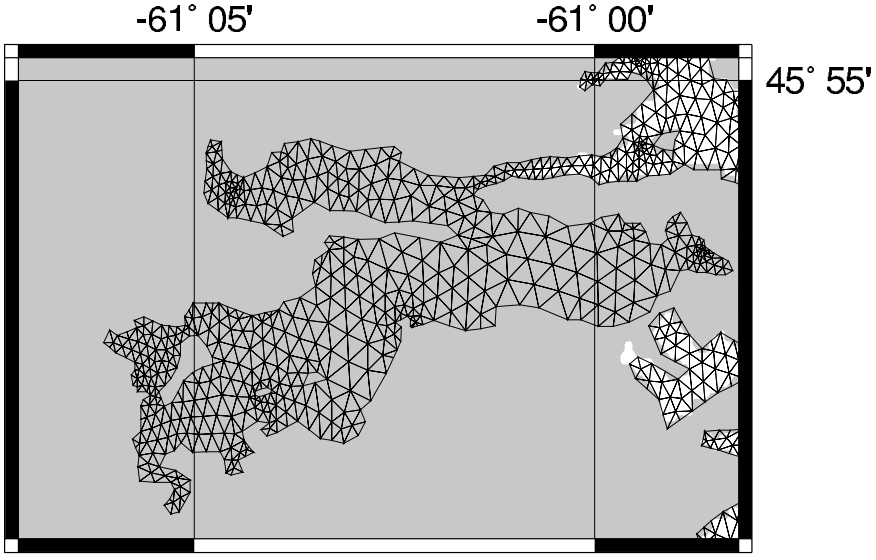

Figure 38(b). Finite element mesh for Denys Basin.

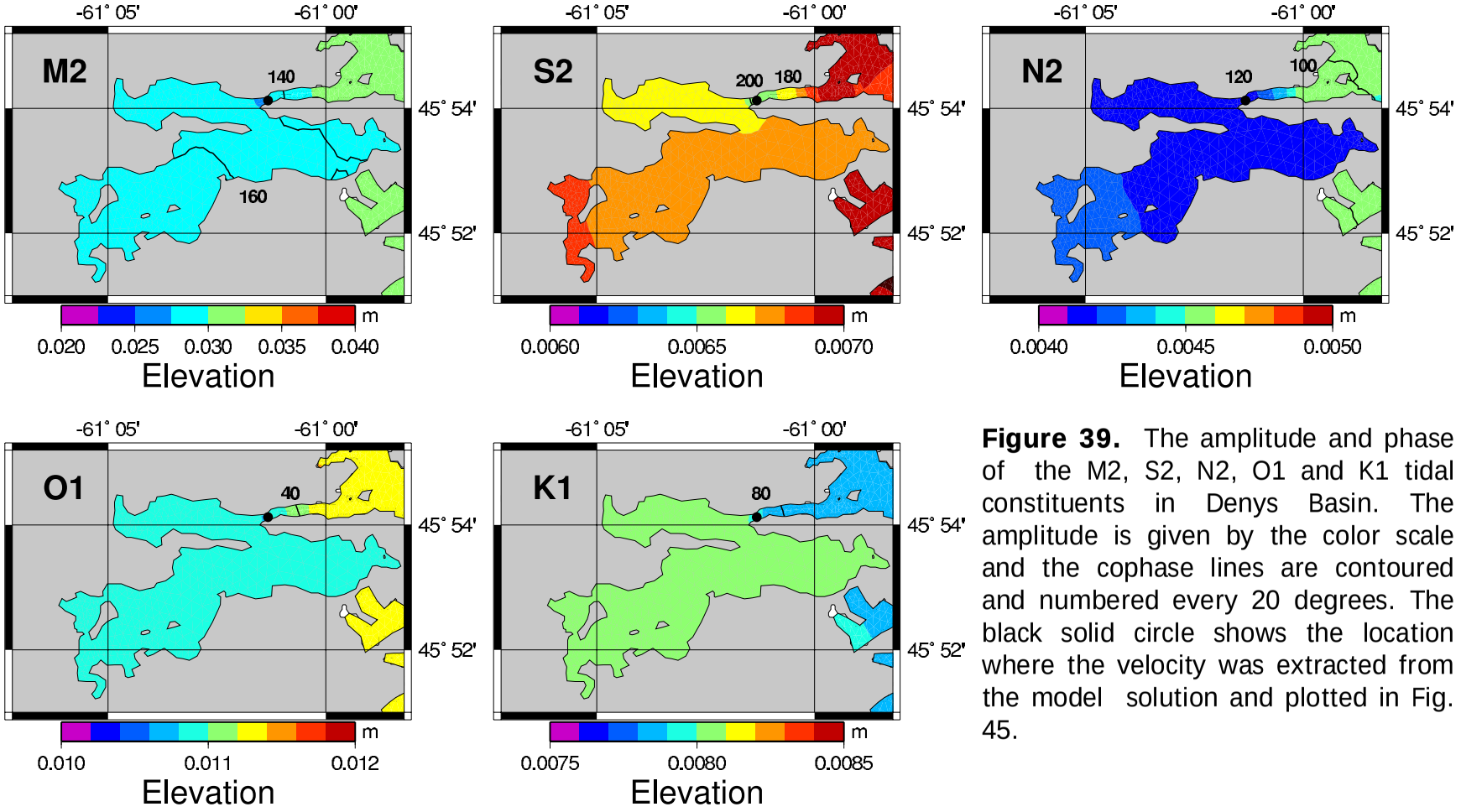

Figure 39. The amplitude and phase of the M2, S2, N2, O1 and K1 tidal constituents in Denys Basin. The amplitude is given by the color scale and the cophase lines are contoured and numbered every 20 degrees. The black solid circle shows the location where the velocity was extracted from the model solution and plotted in Fig. 45.

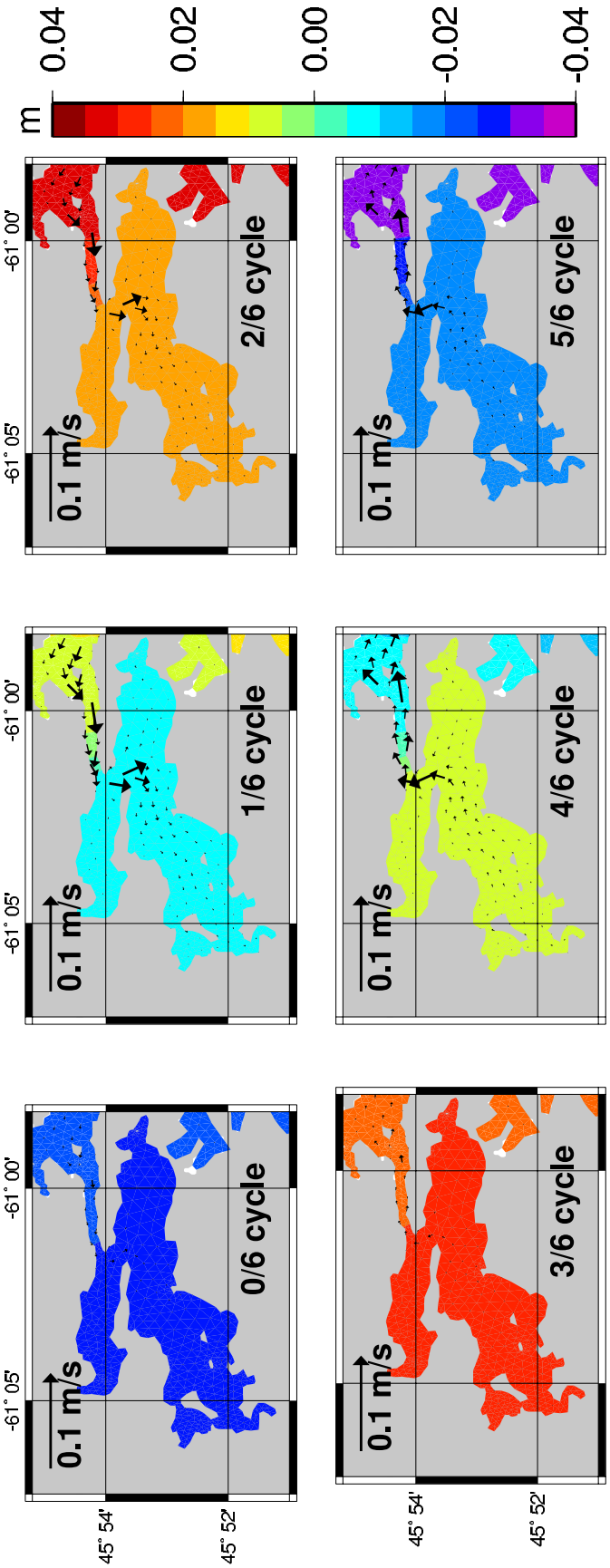

Figure 40. Elevation and currents at 6 stages of the M2 tidal cycle relative to high tide at North Sydney.

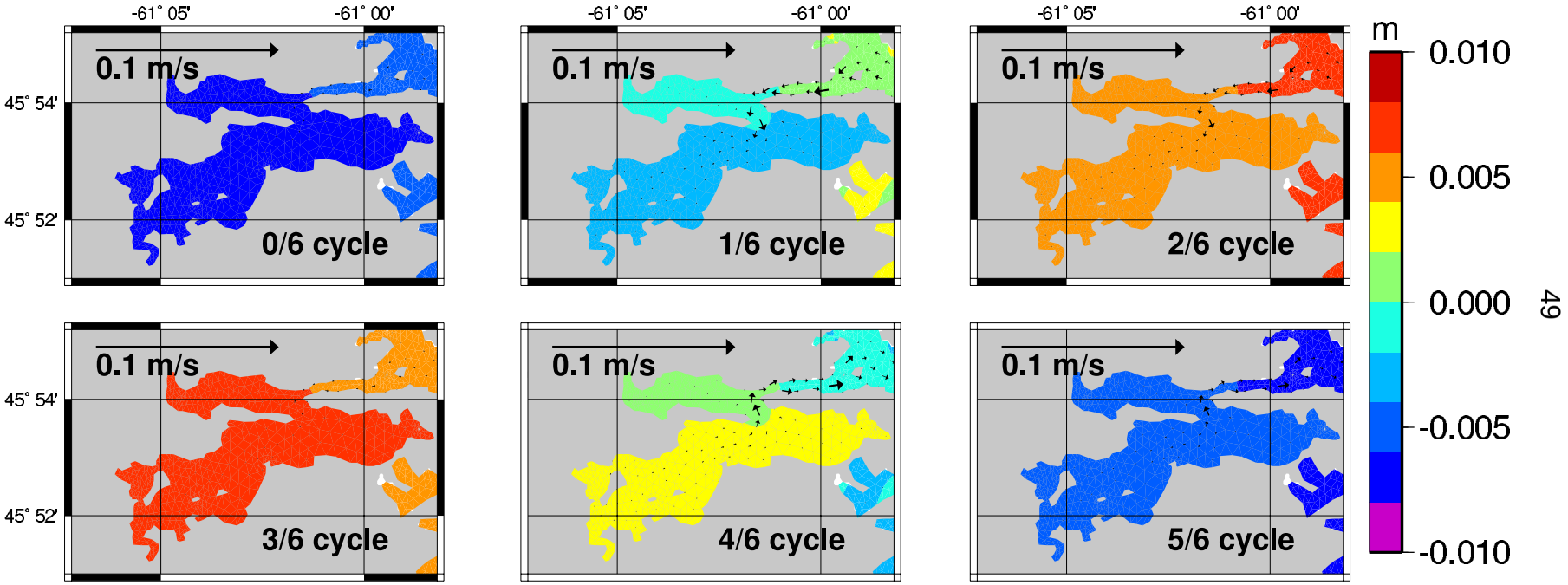

Figure 41. Elevation and currents at 6 stages of the S2 tidal cycle relative to high tide at North Sydney.

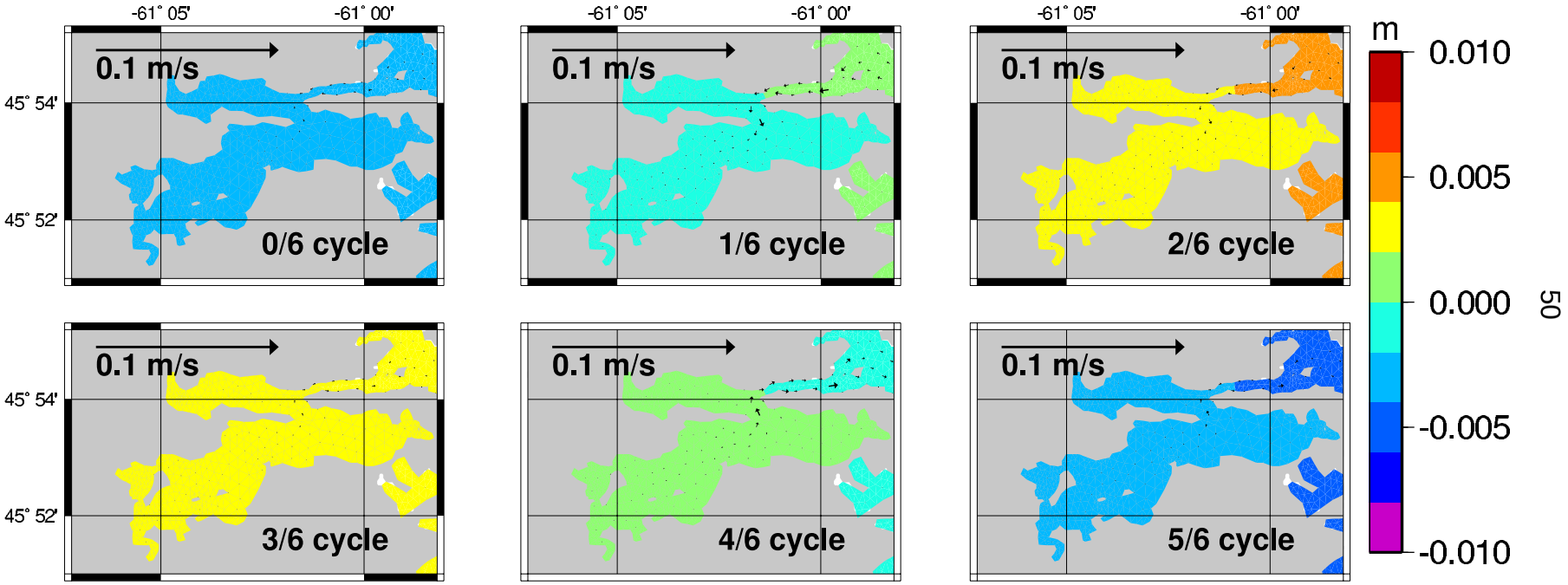

Figure 42. Elevation and currents at 6 stages of the N2 tidal cycle relative to high tide at North Sydney.

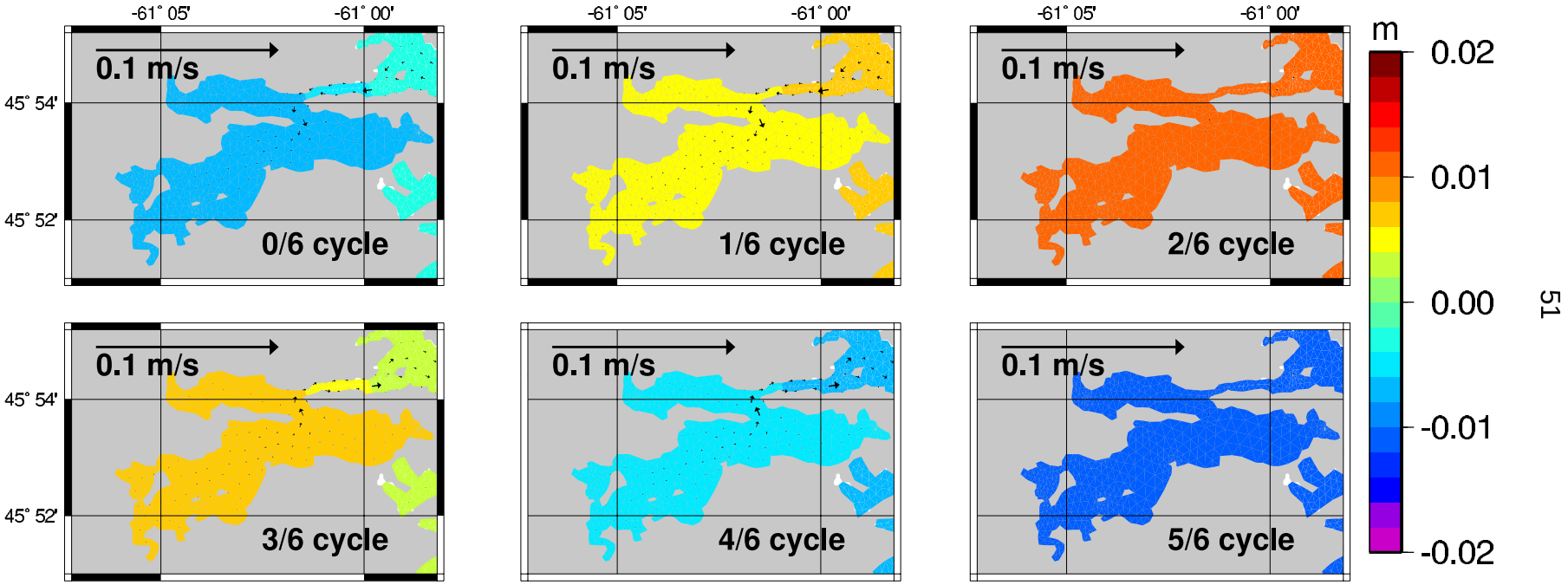

Figure 43. Elevation and currents at 6 stages of the O1 tidal cycle relative to high tide at North Sydney.

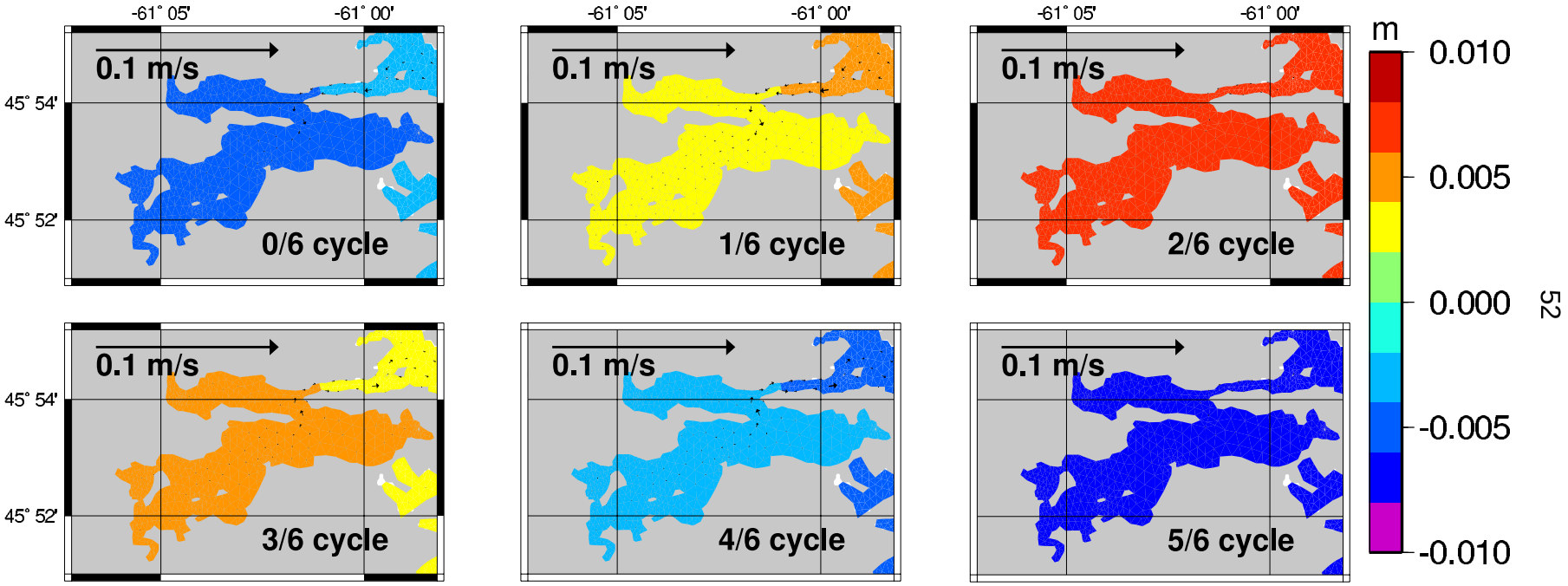

Figure 44. Elevation and currents at 6 stages of the K1 tidal cycle relative to high tide at North Sydney.

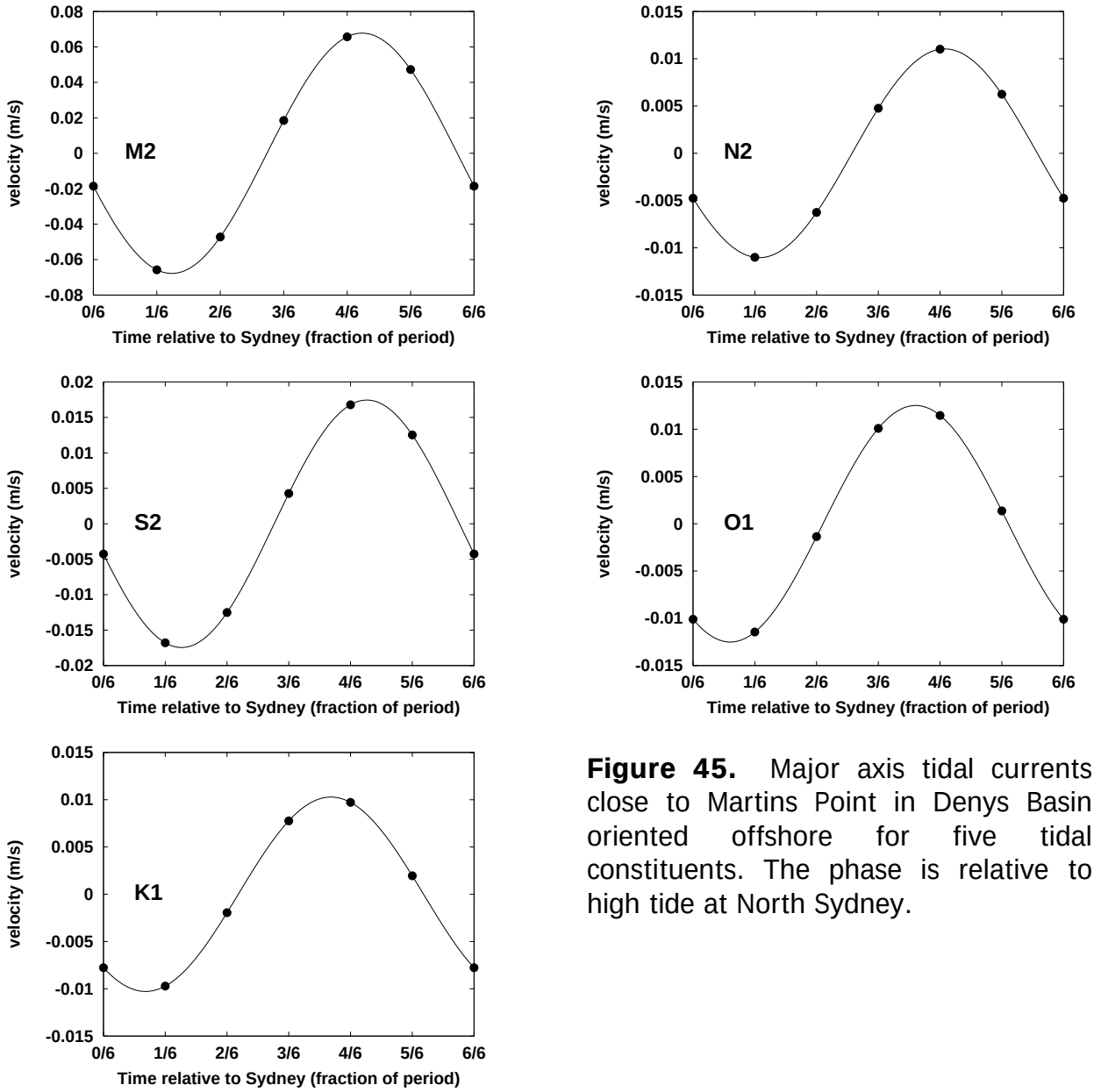

Figure 45. Major axis tidal currents close to Martins Point in Denys Basin oriented offshore for five tidal constituents. The phase is relative to high tide at North Sydney.